

Reply to comments from Dr. Schaefli

1. General comment

1.1 This paper is a re-submission of a paper previously discussed in HESSD. The authors made a considerable effort to revise the text and the model to meet the reviewers' concerns. The model now has a separated degree-day factor for snow and ice and the description of the model is clearer (but still not entirely clear).

Reply: Thanks.

1.2 The proposed step-wise calibration method is tested to show how robust it is if applied to different periods and with different hydrograph separation criteria. The method is certainly transferable to other catchments and interesting for the readership of HESS and I recommend publication in HESS after minor revisions.

Reply: Thanks.

1.3 Before giving some detailed comments hereafter, I would like to point out here that I do not agree with the authors' view that an observed time series can be manipulated such as to "expand the measurement dimension". Information can be extracted from data but the information content of data cannot be increased by any manipulation. Could you please comment on this?

Reply: Thank you for this suggestion. We have modified the related concepts in the paper. 'measurement dimension' has been modified as 'signature dimension' in the revised paper.

Detailed comments:

2. Abstract

2.1 In the abstract, the hydrograph is partitioned according to water sources but then "the hydrological model parameters are grouped by the associated *runoff generation mechanism*"; please use coherent wording according to the very first review of the 1st submission to HESSD. Same holds for section 3, and for the conclusion.

Reply: We have modified the 'runoff generation mechanism' as 'runoff water sources' in the revised paper.

2.2 The abstract does not mention any results, conclusions or outlooks, simply

summarizes the method.

Reply: We have expanded the abstract section by adding more details about the results and conclusions:

“Results show that the proposed calibration approach performed reasonably well. Cross validation and comparison to an automatic calibration method indicated its robustness.”

3. Introduction:

3.1 Good literature summary.

Reply: Thanks.

3.2 I do not agree with wording “hydrograph partitioning is another possible way to expand RM”. The measurement dimension cannot be expanded otherwise than by adding data; hydrograph partitioning might help to extract the meaningful information pieces and to match them with the corresponding parameter groups. This helps in parameter search since the parameters are not trying to match a piece of information which they are not supposed to simulated. But this does not “add measurements” and the measurement dimension is thus not expanded.

Reply: We have done the related modification in the revised paper by replacing the ‘measurement dimension’ with the ‘signature dimension’. Here this sentence has been corrected as “However, glacier mass data and baseflow data are usually not available in some mountain basins. In these cases, hydrograph partitioning is another possible way to exploit information from available data.” in the revised paper.

4. Case study

4.1 I re-iterate my comment: why is the case study qualified as “alpine”? For botany, “alpine” might be a general term referring to any high elevation mountain range, for hydrology, “alpine” refers to my understanding to a hydro-climatic regime with a winter season with snow accumulation and a summer season with melt occurring due to high temperatures; is this the case here? Or do we have a regime where accumulation and melt occur both during the summer as in the Himalaya? On web of science, I could find a single paper mentioning the words “alpine hydrology and Tianshan”. Could you not just say why the area has alpine hydrology? Or simply replace alpine area by mountainous area? Namely also on p. 13398 and 13399 where

the more general “mountainous area” should be used instead of alpine.

Reply: To the authors’ understanding, the term ‘alpine’ is an alternative word (and short) for high mountain area. It has no hydrological meaning in this manuscript as referred by the Referee. Thanks for your suggestion. To avoid misunderstanding, we have replaced all the word “alpine” with the word “mountain” or “mountainous” in the revised paper.

5. Method

5.1 I still do not understand how you connect the accumulation and melt of snow with the modis image. The paper says that snow accumulation and potential melt are simulated per subcatchment, I conclude that SWE is also computed per subcatchment. How do you connect this to the area that experiences melt as obtained from the MODIS image? Do you multiply the potential melt (mm/day) with the area that experiences melt? But then, how do you update the SWE? What do you do if your computed SWE is non-zero but the MODIS image does not show any snow pixels? And what if SWE is zero but MODIS shows snow?

Reply: In response to this comment, we have added the below discussion in the revised paper:

“To be noted, snowfall in each subcatchment is calculated according to the daily precipitation and temperature. And snowmelt is simulated using the degree-day method. However, the snow water equivalent in the snow cover zone (non-glacier area) is not computed. The existing of snow cover in each subcatchment is only determined by MODIS snow image. When the MODIS image indicates the existing of snow cover and meanwhile the daily temperature is higher than 0 °C, then snowmelt will occur, otherwise, snowmelt will not occur. The identification of snow cover by MODIS image is in accordance with the fact that the partitioning of snowmelt dominant hydrograph is based on MODIS snow products. If the existing of snow cover is determined by snow water equivalent, the temperature parameters to calculate snowfall can have significant effects on the estimation of the degree-day factor for snowmelt. To partly reduce this effect, we calibrate the degree-day factor for snowmelt on the basis of MODIS snow cover products. Although in this way, the water balance of snow cover is not taken into account in the snow cover zone, it should not impact the calibration of the degree-day factor for

snowmelt.”

5.2 The use multi-letter parameter names is banned by HESS.

Reply: Thanks, we have modified all the multi-letter parameter names into subscripts.

‘KKA’ is corrected to ‘K_A’, ‘KKD’ is corrected to ‘K_D’ and ‘WM’ is corrected to ‘W_M’.

6. Results

6.1 I recommend explicitly commenting on the fact that clearly, the automatic calibration cannot find the solution to the optimization problem, otherwise it *HAS* to find a solution that is better than the step-wise solution. If the automatic solution found by optimizing NSE has a lower NSE or higher RMSE than the manual calibration, this means that the algorithm could not find the optimum.

Reply: In response to this comment, we have added the discussion below in the revised paper:

“It is worth noting, the performance of the automatic calibration algorithm can increase if the algorithm keeps on running, and even get higher performance than the step-wise calibration method. The comparison here is intending to show that the step-wise calibration method based on hydrograph partition can achieve considerable performance more effectively. The automatic algorithm here treats all the parameters equally during the calibration period. Each parameter should be optimized when searching for the optimal parameter set. This searching algorithm hampers the efficiency of the calibration procedure without identifying the dominant sub-periods for different parameters. In the step-wise calibration method, only parameters that are responsible for the simulation of corresponding hydrograph partition are optimized in each step. And also the calibration of parameter by this method reflects the role of each parameter for the basin runoff generation.”

6.2 Again, I do not agree with the wording “Benefitting from the partitioning curves, however, the stepwise calibration method increases the dimension of measurement information to four. The measurement dimension is now equal to the number of parameter groups,” The information content of data cannot be expanded by data manipulation. It can only be extracted. Otherwise you would create information.

Reply: In the revised paper, we have revised this sentence as “Benefitting from the

partitioning curves, however, the stepwise calibration method increases the dimension of hydrological signature to four. The signature dimension is now equal to the number of parameter group.”

6.3 What means “to extracting index information”?

Reply: it have been corrected as “to extract hydrological signatures”.

Reply to comments from Dr. Zappa

1. Remarks:

1.1 This manuscript is a re-submission of I manuscript I already evaluated in March 2014. The original manuscript was already rather interesting concerning topic and concepts, but rather unripe in its realization, analysis and presentation. In this new version the problematic issues have been addressed.

Reply: Thanks.

1.2 In its current form the paper is very well embedded in scientific literature on the topic. Also the description of the test area is well documented and referenced. As in the original manuscript I appreciate the use of field data for estimating the lapse rates (Sections 2.2.1 and 2.2.2). This is a nice example of confining uncertainty by adding additional information from observations.

Reply: Thanks.

1.3 Concerning the improvements we have now in Table 5 a good overview including calibration and evaluation periods.

Reply: Thanks.

1.4 In the original submission I was complaining because I found your model was not able to capture peaks due to storm rainfall and rapid reaction by the basin. In this version I found this issue is almost solved. Did you some adjustments in the process description? Or is this an improvement stemming from the changes in the snowmelt and icemelt components (Page 13402)?

Reply: The model has been slightly modified in Section 3.2. We have improved the process for runoff generated from rainfall directly in glacier area in the model. Given the relative large glacier coverage and the steep terrain in the study basin, rainfall provides storm runoff and flows into the stream network directly, which flows into the bare soil zone and reaches the stream network slowly in the previous model. The simulation of peak flows have been improved significantly benefiting from these modifications.

2. Points to be addressed:

2.1 I already mentioned in the original submission, that you should be careful in defining your partition a “dominant runoff mechanism”. In this manuscript you

confuse and mix this again. I remember we suggested to use “dominant source of water”.

Reply: Thanks. We have modified all the ‘runoff generation mechanism’ as ‘runoff water sources’ in the revised paper.

2.2 On page 13400 you present your rules to separate the hydrograph. In Figure 6 we see the temporal distribution of the 4 options presented in Eq. 6. I understand you want to keep the rules easy, but if I correctly interpret Figure 6 you have surely small rain events in April. The red and green categories are very marginal in your test area, as they should focus on temperature driven snow and icemelt short before and short after the rain season. How do these rain events with obvious generation of Q_r affect your calibrated data sets?

Reply: Given the seasonality of precipitation in our test area (shown in Figure 3), we neglected the rain events in the period from October to April for the test of the proposed calibration method. We acknowledge that this is a rough assumption, and surely small rain events will occur during this period. To take the effects of these rain events on the calibration into account, an iteration calibration procedure is adopted in this study. The parameters for melt and rainfall runoff are firstly calibrated on their dominant hydrograph parts (red and green, blue in Figure 6) separately, then the melt parameters are re-calibrated on the basis of the calculation of rainfall runoff using the parameters already calibrated in the first step. This calibration procedure is repeated until the parameter values getting a stable level. In this way, the effects of rainfall events in April on the calibration can be partly taken into account. And also, we have done some work to evaluate the sensitivity of the calibration to the partition of the rainfall event dominant hydrograph in Section 4.5. Results in Table 6 and Figure 10 show the rainfall events can have an important role on the calibration on the rainfall runoff parameter (i.e. W_M), while have relatively slighter effects on the calibration of melt and groundwater parameters. The accurate partition of the rainfall runoff dominant hydrograph should be improved based on the more accurate measurement of rainfall in the test area, which can be working for further study.

2.3 13403: As table 6 demonstrate their sensitivity to your approach, can you give some

more information on the meaning of KKA and KKD. You call both of them “coefficient used to calculate calibrated subsurface flow”, which is for me no useful information. Are the two factors linkable to some physical property (infiltration, storage coefficient or so?)

Reply: We have added the below sentence in Section 3.2 in the revised manuscript:

K_A and K_D are outflow coefficients of groundwater storage. Their sum determines the flow rate of groundwater baseflow and their ratio (K_D / K_A) dominate the proportion of free groundwater storage. Infiltration and storage should have effects on the calibration of the two parameters.

3. Minor issues:

3.1 13390-15: Typo: “slope”

Reply: We have revised it.

3.2 13400: The notation chosen in Equation 6 is rather odd (minus signs in the indices to describe the mathematical equivalence). It is surely how you implemented it in your algorithm, but it is not very elegant in a manuscript. Wouldn't be better to have maybe a table instead?

Reply: We have improved it in the form as follow in the revised manuscript:

$$Q = \begin{cases} Q_{SB} & \text{for } S_i=0, G_i=0, \text{ and } D_i = 0 \\ Q_{SB} + Q_{SM} & \text{for } S_i=1, G_i=0, \text{ and } D_i = 0 \\ Q_{SB} + Q_{SM} + Q_{GM} & \text{for } S_i=1, G_i=1, \text{ and } D_i = 0 \\ Q_{SB} + Q_{SM} + Q_{GM} + Q_R & \text{for } D_i = 1 \end{cases}$$

3.3 Table 3: on which basis you decide to have identical hydraulic conductivity in the u-zone and s-zone?

Reply: The soil layer in the test area is very thin. Soil storage capacity is relative low. Subsurface flow is mainly generated from groundwater. To make the simulation of subsurface flow simple, we assumed the hydraulic conductivity of the u-zone is same to the s-zone.

Final considerations:

I thank the authors for having made the effort to invest some more time to improve this manuscript. I listen now only few point they should now address. If this is achieved then

I can recommend the paper for acceptance.

Reply: Thanks. The related points have been addressed in the revised manuscript.

List of relevant changes (in the markup manuscript)

1. In response to the No. 1.3 comment from Dr. Schaepli, we have modified the related “measurement dimension” as “signature dimension”.
2. In response to the No. 2.1 comment from Dr. Schaepli, all the “runoff generation mechanism” have been modified as “runoff water sources”.
3. In response to the No. 2.2 comment from Dr. Schaepli, we have added the words “Results show that the proposed calibration approach performed reasonably well. Cross validation and comparison to an automatic calibration method indicated its robustness” on line 44-46 in the revised manuscript.
4. In response to the No. 3.2 comment from Dr. Schaepli, we have corrected this sentence as “However, glacier mass data and baseflow data are usually not available in some mountain basins. In these cases, hydrograph partitioning is another possible way to exploit information from available data” on line 168-170 in the revised manuscript.
5. In response to the No. 4.1 comment from Dr. Schaepli, we have corrected all the “alpine” as “mountain” or “mountainous”.
6. In response to the No. 5.1 comment from Dr. Schaepli, we have added the below sentences on line 483-499 in the revised manuscript to describe the model in more detail.

“To be noted, snowfall in each subcatchment is calculated according to the daily precipitation and temperature. And snowmelt is simulated using the degree-day method. However, the snow water equivalent in the snow cover zone (non-glacier area) is not computed. The existing of snow cover in each subcatchment is only determined by MODIS snow image. When the MODIS image indicates the existing of snow cover and meanwhile the daily temperature is higher than 0 °C , then snowmelt will occur, otherwise, snowmelt will not occur. The identification of snow cover by MODIS image is in accordance with the fact that the partitioning of snowmelt dominant hydrograph is based on MODIS snow products. If the existing of snow cover is determined by snow water equivalent, the temperature parameters to calculate snowfall can have significant effects on the estimation of the degree-day factor for snowmelt. To partly reduce this effect, we calibrate the degree-day factor for snowmelt on the basis of MODIS snow cover products. Although in this way, the water balance of snow cover is not taken into account in the snow cover zone, it should not impact the calibration of the degree-day factor for snowmelt.”
7. In response to the No. 5.2 comment from Dr. Schaepli, we have corrected all the multi-letter parameter names into subscripts, i.e., ‘ KKA ’ is corrected to ‘ K_A ’, ‘ KKD ’ is corrected to ‘ K_D ’ and ‘ WM ’ is corrected to ‘ W_M ’.

8. In response to the No. 6.1 comment from Dr. Schaepli, we have added a paragraph below on line 658-668 in the revised manuscript to discuss the automatic calibration algorithm.

“It is worth noting, the performance of the automatic calibration algorithm can increase if the algorithm keeps on running, and even be higher than that of the step-wise calibration method. The comparison here is intending to show that the step-wise calibration method based on hydrograph partition can achieve considerable performance more effectively. The automatic algorithm here treats all the parameters equally during the calibration period. Each parameter should be optimized when searching for the optimal parameter set. This searching algorithm hampers the efficiency of the calibration procedure without identifying the dominant sub-periods for different parameters. In the step-wise calibration method, only parameters that are responsible for the simulation of corresponding hydrograph partition are optimized in each step. And also the calibration of parameter by this method reflects the role of each parameter for the basin runoff generation.”
9. In response to the No. 6.2 comment from Dr. Schaepli, we have corrected this sentence as “Benefitting from the partitioning curves, however, the stepwise calibration method increases the dimension of hydrological signature to four. The signature dimension is now equal to the number of parameter groups, and the grouped parameters can be optimized according to their corresponding runoff components separately” on line 642-645 in the revised manuscript.
10. In response to the No. 6.3 comment from Dr. Schaepli, we have corrected these words as “to extract hydrological signatures” on line 797 in the revised manuscript.
11. In response to the No. 2.1 comment from Dr. Zappa, we have corrected all the “runoff mechanism” as “runoff water sources”.
12. In response to the No. 2.2 comment from Dr. Zappa, we have added the discussion “Given that the hydrograph partition in Fig. 6 is on the basis of setting the SRP as May to September, some small rain events in April are not taken into account. Sensitive analysis in Table 6 indicates that taking these events into account (i.e., defining SRP as April to October and April to September), the calibrated value of parameter W_M can be significantly different” on line 751-755 in the revised manuscript.
13. In response to the No. 2.3 comment from Dr. Zappa, we have added these sentence “ K_A and K_D are outflow coefficients of groundwater storage. Their sum determines the flow rate of groundwater baseflow and their ratio (K_D/K_A) dominate the proportion of free groundwater storage. Infiltration and storage should have effects on the calibration of the two parameters.” on line 460-463 in the revised manuscript.
14. In response to the No. 3.1 comment from Dr. Zappa, the word has been corrected as “slope”

on line 150 in the revised manuscript.

15. In response to the No. 3.2 comment from Dr. Zappa, the format of equation 6 has been corrected below on line 415 in the revised manuscript.

$$Q = \begin{cases} Q_{SB} & \text{for } S_i=0, G_i=0, \text{ and } D_i = 0 \\ Q_{SB} + Q_{SM} & \text{for } S_i=1, G_i=0, \text{ and } D_i = 0 \\ Q_{SB} + Q_{SM} + Q_{GM} & \text{for } S_i=1, G_i=1, \text{ and } D_i = 0 \\ Q_{SB} + Q_{SM} + Q_{GM} + Q_R & \text{for } D_i = 1 \end{cases}$$

1 **Diagnostic calibration of a hydrological model in a mountain**
2 **area by hydrograph partitioning**

Deleted: an alpine

3 Z. H. He¹, F. Q. Tian^{1*}, H. V. Gupta², H. C. Hu¹, H. P. Hu¹

4
5
6 1. State Key Laboratory of Hydrosience and Engineering, Department of Hydraulic
7 Engineering, Tsinghua University, Beijing 100084, China

8 2. Department of Hydrology and Water Resources, The University of Arizona, Tucson,
9 Arizona, 85721, USA

10
11 *Corresponding author information:

12 Email: tianfq@tsinghua.edu.cn

13 Tele: +86 010 6277 3396

14 Fax: +86 010 6279 6971

15
16
17
18 Manuscript submitted to Hydrology and Earth System Sciences

19 2015.03.02

20 Deleted: 2014.10.27

23 **Abstract**

24 Hydrological modeling can exploit informative signatures extracted from long time sequences
25 of observed streamflow for parameter calibration and model diagnosis. In this study we
26 explore the diagnostic potential of hydrograph partitioning for model calibration in mountain,
27 areas, where meltwater from snow and glaciers are important sources for river runoff (in
28 addition to rainwater). We propose an index-based method to partition the hydrograph
29 according to dominant runoff water sources, and a diagnostic approach to calibrate a
30 mountain hydrological model. First, by accounting for the seasonal variability of precipitation
31 and the altitudinal variability of temperature and snow/glacier coverage, we develop a set of
32 indices to indicate the daily status of runoff generation from each type of water source (i.e.,
33 glacier meltwater, snow meltwater, rainwater, and groundwater). Second, these indices are
34 used to partition a hydrograph into four parts associated with four different combinations of
35 dominant water sources (i.e., groundwater, groundwater + snow meltwater, groundwater +
36 snow meltwater + glacier meltwater, groundwater + snow meltwater + glacier meltwater +
37 rainwater). Third, the hydrological model parameters are grouped by the associated runoff
38 sources, and each group is calibrated to match the corresponding hydrograph partition in a
39 stepwise and iterative manner. Similar to use of the regime curve to diagnose seasonality of
40 streamflow, the hydrograph partitioning curve based on a dominant runoff water source (more
41 briefly called the partitioning curve, not necessarily continuous) can serve as a diagnostic
42 signature that helps relate model performance to model components. The proposed methods
43 are demonstrated via application of a semi-distributed hydrological model (THREW) to the
44 Tailan River basin (1324 km²) in the Tianshan Mountain of China. Results show that the
45 proposed calibration approach performed reasonably well. Cross validation and comparison to
46 an automatic calibration method indicated its robustness.

Deleted: alpine

Deleted: an alpine

Deleted: generation mechanism

50 **1 Introduction**

51 **1.1 Background**

52 Parameter calibration has been singled out as one of the major issues in the application
53 of hydrological models (Johnston and Pilgrim, 1976; Gupta and Sorooshian, 1983; Beven and
54 Binley, 1992; Boyle *et al.*, 2000). Commonly, one or more objective functions are selected as
55 criteria to evaluate the similarity between observed and simulated hydrographs (Nash and
56 Sutcliffe, 1970; Brazil, 1989; Gupta *et al.*, 1998; van Griensven and Bauwens, 2003). As
57 model complexity increases, parameter dimensionality also increases significantly, which
58 makes it much more difficult to calibrate model parameters manually. For this reason,
59 automatic calibration procedures have been developed to identify the optimal parameter set
60 (Gupta and Sorooshian, 1985; Gan and Biftu, 1996; Vrugt *et al.*, 2003a,b). However, due to
61 limitations in process understanding and measurement technologies, one can find different
62 parameter sets within a chosen space that may acceptably reproduce the observed aspects of
63 the catchment system (Sorooshian and Gupta, 1983; Beven and Freer, 2001). This
64 phenomenon, which has been called “equifinality”, causes uncertainty in simulation and
65 prediction (Duan *et al.*, 1992; Beven, 1993, 1996), and highlights the need for methods that
66 are powerful enough to ‘diagnostically’ evaluate and correct models, i.e., that are capable of
67 indicating to what degree a realistic representation of the real world has been achieved and
68 pointing towards how the model should be improved (Spear and Hornberger, 1980; Gupta *et al.*,
69 1998, 2008).

70 Traditional regression-based model evaluation strategies (e.g., based on the use of Mean
71 Squared Error or Nash Sutcliffe Efficiency as performance criteria) are demonstrably poor in
72 their ability to identify the roles of various model components or parameters in the model
73 output (Van Straten and Keesman, 1991; Zhang *et al.*, 2008; Gupta *et al.*, 2008; Yilmaz *et al.*,
74 2008; Hingray *et al.*, 2010), which is due in part to the loss of meaningful information when
75 projecting from the high dimension of the data set (like hydrograph) down to the low (often
76 one) dimension of the measure (Yilmaz *et al.*, 2008; Gupta *et al.*, 2009). A diagnostic
77 evaluation method should match the number of unknowns (parameters) with the number of
78 pieces of information by making use of multiple measures of model performance (Gupta *et al.*,
79 1998, 2008, 2009; Yilmaz *et al.*, 2008). One way to exploit hydrological information is to

80 analyze the spatiotemporal characteristics of hydrological variables that can be related to
81 specific hydrological processes in the form of “signature indices” (Richter *et al.*, 1996;
82 Sivapalan *et al.*, 2003; Gupta *et al.* 2008, Yilmaz *et al.*, 2008). Ideally, a “signature” should
83 represent some “invariant” property of the system, be readily identifiable from available data,
84 directly reflect some system function, and be maximally related to some “structure” or
85 “parameter” in the model.

86 Attention to hydrological signatures, therefore, constitutes the natural basis for model
87 diagnosis (Gupta *et al.*, 2008). Placed in this context, the body of literature on the topic is
88 indeed large. Jothityangkoon *et al.* (2001) proposed a downward approach to evaluate the
89 model’s performance against appropriate signatures at progressively refined time scale.
90 Signatures that govern the evaluation of model complexity are the inter-annual variability,
91 mean monthly variation in runoff (called regime curve), and the flow duration curve (FDC).
92 Farmer *et al.* (2003) evaluated the climate, soil and vegetation controls on the variability of
93 water balance through four signatures: gradient of the annual yield frequency graph, average
94 yield over many years for each month, FDC, and magnitude and shape of the hydrograph.
95 Shamir *et al.* (2005a) described a parameter estimation method based on hydrograph
96 descriptors (total flow, range between the extreme values, monthly rising limb density of the
97 hydrograph, monthly maximum flow and negative/positive change) that characterize
98 dominant streamflow patterns at three timescales (monthly, yearly, and record extent).
99 Detenbeck *et al.* (2005) calculated several hydrologic indices including daily flow indices
100 (mean, median, coefficient of variation, and skewness), overall flood indices (flood frequency,
101 magnitude, duration, and flood timing of various levels), low flow variables (mean annual
102 daily minimum), and ranges of flow percentiles to study the relationship of the streamflow
103 regime to watershed characteristics. Shamir *et al.* (2005b) presented two streamflow indices
104 to describe the shape of the hydrograph (rising/declining limb density, i.e., RLD and DLD)
105 for parameter estimation in 19 basins of United States. Yadav *et al.* (2007) used similarity
106 indices and hydrological signatures (runoff ratio and slope of the FDC) to classify catchments.
107 Westerberg *et al.* (2011) selected several evaluation points on the FDC to calibrate models,
108 and compared two selection methods to evaluate their effects on parameter calibration.

109 Generally, the reported signatures have the following two characteristics: (1) they

110 concentrate on the extraction of hydrologically meaningful information contained in
111 hydrographs, and (2) they focus on either an entire study period or a special continuous
112 section of the entire period. They have occasionally considered temporal variability of runoff
113 components and dominance of different runoff sources during different periods (e.g., the
114 seasonal switching of runoff sources discussed in Tian *et al.*, 2012). However, a hydrograph
115 could be dominated by various components or water sources at different response times
116 (Haberlandt *et al.*, 2001; Eder *et al.*, 2005). Within this in mind, a few studies have explored
117 the use of hydrological information in time dimension for stepwise calibration. For example,
118 Schaefli *et al.* (2005) presented a stepwise calibration method for 7 parameters in a high
119 mountainous area: snow and ice melt degree-day factors were conditioned by mass balance,
120 slow reservoir parameters were determined by base flow, reservoir coefficients were
121 calibrated by summer runoff, and the direct runoff coefficient was used to control discharge
122 during precipitation events. Another notable example is Hingray *et al.* (2010), in which the
123 authors estimated the value of snowmelt degree-day factor in a mountain basin by
124 progressively minimizing the differences between observed and simulated values of different
125 magnitude hydrographs. There are also many other follow up studies.

126 In mountain areas, streamflow is composed of both snow/glacier meltwater and
127 rainwater. The energy-based and temperature-index models are two principal approaches to
128 simulate snow and glacier melt (Rango and Martinec, 1979; Howard, 1996; Kane *et al.*, 1997;
129 Singh *et al.*, 2000; Fierz *et al.*, 2003). To describe significant heterogeneity of temperature,
130 precipitation, snow, and glacier, distributed hydrological models are generally used for
131 precipitation-runoff modeling in mountain regions (Daly *et al.*, 2000; Klok *et al.*, 2001 etc.).
132 Also, the utilization of remotely sensing products of precipitation and snow cover data in the
133 mountain runoff modeling has become more popular in recent years (Swamy and Brivio, 1997;
134 Akyurek *et al.*, 2011; Liu *et al.*, 2012 etc.). Most of these studies report sound simulation
135 results. However, the need to develop an appropriate calibration strategy for
136 precipitation-runoff modeling in mountain areas remains a key issue for two reasons: first, the
137 hydrological processes are usually more complex (with snow/glacier melt and possibly soil
138 freezing/thawing) than those in warmer areas, which implies a larger dimension of parameter
139 (R^p) in the corresponding hydrological model; second, measured data set useful for model

Deleted: generation mechanisms

Deleted: generation mechanisms

Deleted: alpine

Deleted: alpine

Deleted: alpine

Deleted: alpine

146 identification is usually limited due to a sparse gauge network, which produces a small
147 measurement dimension (R^M) far lower than R^P . To address this problem, related studies are
148 putting effort into two directions. One is to reduce the calibrated R^P by estimating some of the
149 parameters based on basin characteristics *a priori*. For example, Gurtz *et al.* (1999) proposed
150 a parameterization method based on elevation, slope and shading derived from basin terrain.
151 Gomez-Landes and Rango (2002) obtained model parameters of ungauged basins from
152 gauged basins by basin size, proximity of location, and shape similarities. Eder *et al.* (2005)
153 estimated most of the parameters *a priori* from basin physiography before an automatic
154 calibration is applied. The parameterization method may involve some uncertainties but be
155 useful for the determination of insensitive parameters.

156 The second direction is ~~to exploit hydrological information from implicit measure data~~.
157 For instance, Dunn and Colohan (1999) used baseflow data as additional criteria for model
158 evaluation. Mendoza *et al.* (2003) exploited recession-flow data to estimate hydraulic
159 parameters. Stahl *et al.* (2008) used glacier mass balance information combined with stream
160 hydrographs to constrain melt factors. Huss *et al.* (2008) used annual ice volume change data
161 for optimizing melt and radiation factors, and glacier equilibrium line altitude for
162 precipitation correction factors. Schaepli and Huss (2011) integrated the seasonal information
163 of point glacier mass balance for model calibration by modifying the GSM-SOCONT model.
164 Jost *et al.* (2012) introduced glacier volume loss calculated by high-resolution digital
165 elevation models to calibrate hydrologic model. Knowledge acquired from the
166 aforementioned research indicates that the use of additional information (e.g., baseflow,
167 recession flow, and glacier mass balance) can effectively help reduce parameter uncertainty.

168 ~~However, glacier mass data and baseflow data are usually not available in some~~
169 ~~mountain basins. In these cases, hydrograph~~ partitioning is another possible way to ~~exploit~~
170 ~~information from available data~~. Information about dominant hydrological processes
171 contained in a hydrograph can be extracted by hydrograph partitioning or separation; this has
172 long been a topic of interest in hydrology. Several different kinds of methods have been
173 proposed (Pinder and Jones, 1969; McCuen, 1989; Nathan, 1990; Arnold *et al.*, 1995, 1999;
174 Vivoni *et al.*, 2007), which can generally be classified into graphical methods, analytical
175 methods, empirical methods, geochemical methods and automated program techniques

Deleted: to expand R^M by exploiting

Deleted: available data

Deleted: by significantly expanding R^M

Deleted: Hydrograph

Deleted: expand R^M

181 (Nejadhashemi *et al.*, 2009). Most of them primarily focus on the partitioning of baseflow and
182 are not capable of identifying more than two components. With the advent of isotope methods,
183 multi-component hydrograph separation models have been developed. However, these models
184 need be run for an extended period of time (usually a minimum of one hydrologic year) for
185 the assumption that the isotopes of components are conserved to hold (Hooper and
186 Shoemaker, 1986) and call for volumes of field data that are seldom available in poorly
187 gauged and difficult to access mountain basins.

Deleted: alpine

188 1.2 Objectives and Scope

189 This paper explores the benefits of partitioning the hydrograph into several parts, each
190 related to one combination of dominant water sources for runoff generation. The parameter
191 group controlling each type of runoff generation is then calibrated using the corresponding
192 partitioning hydrographic curves via a stepwise approach, and model deficiencies are
193 diagnosed by evaluating the model simulations associated with each partitioning curve (as a
194 diagnostic signature). We demonstrate the potential of this approach in a mountain area where
195 streamflow is the result of complex runoff generation processes arising from combinations of
196 storm events and snow/glacier melt. The influence of each type of water source (groundwater,
197 snow meltwater, glacier meltwater, or rainwater) varies in time and can be determined by an
198 analysis of the dynamic spatiotemporal information in the available data series.

Deleted: an alpine

199 The paper is organized as follows. Section 2 contains a description of the geographic
200 and hydrological characteristics of the study basin, including the main data sources and data
201 preprocessing. Section 3 details the proposed method of hydrograph partitioning and
202 parameter calibration based on a semi-distributed model coupled with the temperature-index
203 method. Section 4 presents the results and discusses the possible sources of uncertainty.
204 Section 5 provides a summary of this study and discusses further applications of the
205 partitioning strategy.

206 2 Study Area and Data

207 2.1 Overview of the Study Area

208 The study mountain area (Tailan River basin, TRB) is on the south slope of the Tianshan
209 Mountain (one of the highest mountain areas in China) in the Xinjiang Uygur Autonomous
210 Region of China and extends from 41° 35'N to 42° 05' N and 80° 04'E to 80° 35'E, covering a

Deleted: alpine

214 drainage area of 1324 km². Elevation ranges from 1600 m to 7100 m a.s.l. with an average
215 value as high as 4100 m a.s.l. Precipitation occurs mainly in summer and rarely in winter, and
216 winter precipitation always comes in the form of snowfall. Snow coverage accumulates in
217 winter and ablates from spring into late summer when it melts away completely; the snow
218 coverage dynamics can be obtained from MODIS data (see Fig. 4). The basin is highly
219 glacierized with approximately 33% of the basin area covered by glacier ice (see Fig. 1). The
220 glacier coverage stretches from approximately 3000 m to 7100 m a.s.l. and exists mainly at an
221 altitude range of 4000 m to 5000 m a.s.l. Glacier melt and snowmelt form runoff as long as
222 the temperature rises above a certain threshold and provide primary sources for downstream
223 discharge.

224 TRB is a heavily studied mountain watershed in northwestern China. The relevant
225 literature (Kang and Zhu, 1980; Shen *et al.*, 2003; Xie *et al.*, 2004; Gao *et al.*, 2011; Sun *et al.*,
226 2012) are reviewed below, and the main conclusions about the hydrometeorological
227 characteristics are summarized as follows:

228 (1) The climate presents strong altitudinal variability. The mean annual precipitation in
229 higher mountain areas is approximately 1200 mm (Kang *et al.*, 1980), while it is
230 approximately only 180 mm in the outlet plain area (Xie *et al.*, 2004). The mean annual
231 temperature ranges from below 0°C in mountain areas to approximately 9°C at the basin
232 outlet (Sun *et al.*, 2012).

233 (2) Meltwater is the principal source of streamflow. Snow and glacier meltwater account
234 for approximately 63% of the annual runoff (Kang *et al.*, 1980). The contribution of rainwater
235 is relatively lower and occurs mainly in the storm rain period (May to September) (Xie *et al.*,
236 2004). Groundwater baseflow is smaller but dominates the streamflow in the winter (January,
237 February and December), during which either rainfall or melt rarely occur (Kang *et al.*, 1980).

238 (3) The TRB river network is a simple fan system. Given large topographic drop and
239 moderate drainage area, the runoff concentration time is no longer than one day (Xie *et al.*,
240 2004). Melting and falling water can quickly flow into the main channel and reach the basin
241 outlet.

242 2.2 Data & Preprocessing

243 The Tailan gauging station (THS, 1602 m a.s.l.) is located the outlet of the watershed,

Deleted: Figure

Deleted: Figure

Deleted: alpine

247 where runoff, precipitation and temperature have been measured since 1957. To collect
248 temperature and precipitation data at higher elevation, two automatic weather stations (AWS,
249 product type TRM-ZS2) were set up in June 2011 (i.e., XT AWS, at 2116 m a.s.l. and TG
250 AWS, at 2381 m a.s.l.). This relatively short record (from July 1, 2011-December 31, 2012)
251 was used to estimate the lapse rate of precipitation and temperature (see below). The Bingtan
252 automatic weather station (BT AWS, at 3950 m a.s.l.) located in an adjacent catchment
253 (Kumalak basin) was used to validate the estimated temperature lapse rates. A digital
254 elevation model (DEM) with a spatial resolution of 30 m was provided by the International
255 Scientific & Technical Data Mirror Site, Computer Network Information Center of the
256 Chinese Academy of Sciences (<http://www.gscloud.cn>). Remotely sensed snow cover area
257 (SCA) data were downloaded from the MODIS website; the MOD10A2 and MYD10A2
258 products were used, both of which have a spatial resolution of 500m and a temporal
259 resolution of eight-days. Daily snow cover data was obtained by linear interpolation of the
260 eight-day data. The China Glacier Inventory (CGI) (Shi, 2008) was used to derive glacier
261 coverage in the TRB. In our experience, most of the snow melts away after the warm summer
262 period and the lowest snow/ice coverage in the year should, therefore, be roughly equal to the
263 glacier coverage. Based on an analysis of filtered MODIS SCA (see Sect. 2.2.3), the lowest
264 values of snow/ice coverage in the study period (2003-2012) are almost the same, which
265 indicates that TRB glacier coverage is relatively stable during the study period. The DEM,
266 river system, gauging stations and glacier distribution are shown in Fig.1.

267 2.2.1 Temperature Lapse Rate

268 Altitudinal distribution of temperature can be estimated through the lapse rate (Rango and
269 Martinec, 1979; Tabony, 1985). According to Aizen *et al.* (2000), rates of temperature
270 decrease with increasing elevation are quite different in various months, and ignoring this
271 difference may lead to significant errors in the simulation of snow accumulation and melt.
272 The lapse rate was therefore estimated for each month. Temperature variations with altitude
273 can be estimated by the following equation, i.e.:

$$274 \quad T = T_o + T_p \cdot (H - h) \quad (1)$$

275 where, T_o is the temperature value at low altitude (THS in this study), and T_p is the

276 temperature lapse rate (usually negative), H and h are the elevation values at high and low
277 positions, i.e., the mean elevation of two AWS and the elevation of THS, respectively. The
278 values of T_p in different months are obtained by minimizing the error function, i.e.:

$$279 \quad \min : z = \sum (T_i - (T_{oi} + T_p \cdot (H - h)))^2 \quad (2)$$

280 where, i indicates the i^{th} day in the analyzed month, T_i is the observed temperature in AWS,
281 which is the mean value of the TG AWS and XT AWS in this study.

282 The temperature series data from July 1, 2011 to December 31, 2012 at THS, TG AWS
283 and XT AWS were used to estimate the temperature lapse rate. The results (Table 1) indicate
284 significant month-to-month variation ranging from $-0.30^\circ\text{C} 100 \text{ m}^{-1}$ in December to -0.86°C
285 100 m^{-1} in August. To validate the temperature lapse rates, the estimated and observed
286 temperature data at BT AWS were compared (Fig. 2). We also compared the estimated
287 temperature by an annual constant lapse rate ($-0.62^\circ\text{C} 100 \text{ m}^{-1}$, a similar value to previous
288 studies, e.g., Tabony (1985) and Tahir *et al.* (2011)). This constant value is optimized by the
289 same method in Eqn. (2) but using all daily temperature measurements. Figure 2 indicates that
290 the monthly lapse rate method performs better than the annual constant rate method at the BT
291 station for all months throughout the year. Further, the temperature curves estimated by
292 monthly lapse rates for April to August match the observed ones rather well. Note that the
293 estimated temperatures tend to underestimate observed ones for the rest of the months, which,
294 however, will not affect the melt runoff significantly due to the general freezing condition
295 during this period.

296 2.2.2 Precipitation Lapse Rate

297 Based on the precipitation series measured at THS, the monthly precipitation to annual
298 precipitation ratio (Fig.3) for the study period (2003-2012) indicates that precipitation occurs
299 mainly in May to September. The lapse rate of precipitation was also estimated monthly, and
300 a similar procedure as temperature was applied. The different is that the precipitation analysis
301 was conducted at a weekly rather than daily time step, and the maximum measured
302 precipitation of the two installed AWS was used instead of the mean value. The analyzed
303 period is limited to the storm rain period (May to September). Other months are not included
304 due to the relatively small precipitation amount. The weekly precipitation lapse rates are

305 listed in Table 2. Daily precipitation differences between higher and lower altitudes can be
306 estimated as the weekly precipitation lapse multiplied by the ratio of daily precipitation to the
307 corresponding weekly amount in THS. The precipitation lapse rate was not validated against
308 BT AWS because of significant differences in precipitation distribution between the two
309 basins (i.e., Tailan and Kumalak).

310 **2.2.3 Filtering of MODIS Snow Cover Area Data**

311 Snow cover extent was obtained from MODIS products. The MOD10A2 and MYD10A2
312 products were downloaded from the website <http://reverb.echo.nasa.gov>. In total, we obtained
313 460 eight-day images (two tiles, h23v04 and h24v04) from 2003 to 2012 for each product.
314 Given that the accuracy of the MODIS SCA product is affected by cloud coverage to a
315 significant degree, the remotely sensed images should be filtered to avoid the noise from
316 clouds before using it for hydrological modeling (Ackerman *et al.*, 1998). The following three
317 successive steps are adopted to filter the products based on previous reports (Gafurov and
318 Bardossy, 2009; Wang *et al.*, 2009; Lopez-Burgos *et al.*, 2012):

319 (1) Satellite combination: The snow cover products of two satellites, Terra (MOD10A2)
320 and Aqua (MYD10A2) were combined. As long as the value of a pixel is marked as snow in
321 either satellite, the pixel value is marked as snow.

322 (2) Spatial combination: Inspecting the values of the nearest four pixels around one
323 center pixel marked as cloud, if at least three of the four surrounding pixels are marked as
324 snow, the center pixel is modified as snow.

325 (3) Temporal combination: If one pixel is marked as cloud, its values in the previous and
326 following observations are investigated. If both of the two observed values are snow, then the
327 present value of the same pixel is snow.

328 As an example, the filtered results from year 2004-2005 shown in Fig.4 demonstrate a
329 significant reduction in fluctuation of the SCA products. We find that the lowest values of
330 snow/ice coverage in all years (2003-2012) are relatively stable (from 2003 to 2012 are: 35%,
331 34%, 39%, 36%, 37%, 34%, 41%, 35%, 38%, 39%, showing no obvious trend), which is
332 close to the glacier coverage area (33%) derived from the CGI data mentioned in Sect.2.2. As
333 mentioned before, MODIS snow/ice covered area in later summer is mainly composed of
334 glacier coverage when snow has been melt away completely. The filtered results indicate a

335 relatively stable coverage of glacier in TRB.

336 **2.2.4 Altitudinal Cumulative Melt Curve**

337 The daily temperature of each cell in MODIS SCA images can be estimated by a
338 temperature lapse rate based on its elevation and daily temperature measured at THS. As long
339 as the temperature exceeds a specific threshold value for melt (assumed to be 0°C in this
340 study), a given cell was labeled as an active cell in terms of melt. The land cover type for each
341 cell was classified into glacier, snow, and other land cover according to the CGI and MODIS
342 SCA product. To obtain the area covered by snow only, we subtracted the glacier area in CGI
343 from the SCA (a similar procedure can be found in Luo *et al.*, 2013). When a glacier or snow
344 cover cell is active, it is labeled as a melt cell, and the melt area is computed as the number of
345 active cells multiplied by the area of a cell.

346 Organizing the melt area by elevation from low to high and summing the melt area at
347 each elevation, we can get the altitudinal cumulative melt curve, which can be used to
348 describe the spatiotemporal distribution of melt area. The altitudinal cumulative melt curves
349 calculated from 2003 to 2012 for all months (Fig.5) show that melt mainly occur from May to
350 September, which coincides with the precipitation period. Snowmelt starts at an elevation of
351 approximately 1650 m a.s.l., while glacier melt starts at an elevation of approximately 2950 m
352 a.s.l, which has an important implication for hydrograph partitioning.

353 **3 Methodology**

354 Theoretically, every drop of water in the streamflow comes ultimately from precipitation.
355 Practically, we can consider water sources for runoff generation in mountain areas as mainly
356 consisting of meltwater from snow and glacier, rainwater, and groundwater. Groundwater at
357 the basin scale is recharged by direct infiltration and run-on infiltration of meltwater or
358 rainwater, and it is mainly discharged as baseflow via a subsurface flow path (especially in
359 mountain areas where the large elevation gradient favors baseflow discharge). For the purpose
360 of hydrograph partitioning, we can consider recharge to be a separate water source for
361 streamflow, independent of meltwater and rainwater, which principally forms the baseflow
362 part of a hydrograph. The remaining part of a hydrograph is principally formed by meltwater
363 and rainwater via surface flow path (Blöschl *et al.*, 2013). We develop three indices to
364 indicate the water sources for runoff generation at the daily time scale. The hydrograph is

Deleted: alpine

Deleted: alpine

367 further partitioned into several sub-parts based on the indices values. Each sub-part is
368 dominated by one or more water sources for runoff generation. With the partitioning
369 hydrographic curves, the parameters of hydrological models are correspondingly grouped by
370 runoff ~~sources~~, and calibrated in a stepwise fashion. We use the THREW model coupled with
371 a temperature-index module as an exploratory tool. To better demonstrate usefulness of the
372 proposed methods, only the runoff generation related parameters, which are also significantly
373 sensitive parameters (see Sect.4.6), are calibrated. Other insensitive parameters are fixed at
374 their initial values, specified *a priori* from the literature or by expert knowledge.

375 3.1 An Index-based Method for Hydrograph Partitioning

376 In ~~mountain~~ areas, the relative contribution of different runoff water sources to the total
377 streamflow varies throughout the year (Martinec *et al.*, 1982; Dunn and Colohan, 1999; Yang
378 *et al.*, 2007). For the rainwater source, Fig. 3 shows that precipitation in TRB presents strong
379 seasonality and primarily concentrates (more than 76%) in the storm rain period from May to
380 September. During the relatively dry period from October to April, mean precipitation gauged
381 at the THS is just 43 mm, while precipitation in the higher mountainous region is mainly
382 snowfall. Therefore, surface runoff induced by rainwater can rarely occur during relative dry
383 period. It is reasonable to assume that the rainwater source can only contribute to the surface
384 runoff part of a hydrograph on the same day during the storm rain period (May to September)
385 except for the baseflow occurring much later.

386 For the meltwater sources, the altitudinal cumulative melt curves (Fig. 5) show that the
387 areas experiencing glacier melt and snowmelt change significantly with elevation. Melt of
388 glacier and snow begins at different elevations in different months, i.e., glacier melt can only
389 occur in the areas higher than 2950 m (the lower elevation limit of glacier coverage) while
390 snowmelt can occur in areas higher than 1650 m. It can be deduced that snowmelt generally
391 occurs at lower elevations than glacier melt. Remember that temperature decreases with
392 increase in altitude. There should exist a period of time during which temperature at 1650 m
393 is higher than snowmelt threshold while temperature above 2950 m is lower than glacier
394 threshold and thus snow melt does occur but glacier melt not.

395 The groundwater source should be a dominant source for the baseflow part of a
396 hydrograph and, of course, it dominates the recession limb of a hydrograph (part of a

Deleted: generation mechanisms

Deleted: alpine

399 baseflow partition) when no rainfall or melting occurs.

400 Based on the above physical understanding, we can partition the hydrograph using the
401 following three indices:

402 (1) Date index (D_i): D_i is used to distinguish the dates on which rainfall and thus
403 possible rainwater directly runoff process occurs. For simplicity, in this study we use
404 D_i to distinguish dry period and storm rain period and assume no rainfall runoff in
405 the dry period, i.e.,

$$406 \quad D_i = \begin{cases} 1, & \text{for days in storm rain period from May to September} \\ 0, & \text{for days in relative dry period from October to April} \end{cases} \quad (3)$$

407 (2) Snowmelt index (S_i): S_i indicates whether snowmelt possibly occurs on a
408 given day:

$$409 \quad S_i = \begin{cases} 1, & \text{for days when temperature at altitude 1650 m is higher than } 0 \text{ }^\circ\text{C} \\ 0, & \text{for other days} \end{cases} \quad (4)$$

410 (3) Glacier melt index (G_i): G_i is used to identify days when glacier melt
411 possibly occurs:

$$412 \quad G_i = \begin{cases} 1, & \text{for days when temperature at altitude 2950 m is higher than } 0 \text{ }^\circ\text{C} \\ 0, & \text{for other days} \end{cases} \quad (5)$$

413 The hydrograph is then partitioned according to the three indices by using the following
414 rules:

$$415 \quad Q = \begin{cases} Q_{SB} & \text{for } S_i=0, G_i=0, \text{ and } D_i = 0 \\ Q_{SB} + Q_{SM} & \text{for } S_i=1, G_i=0, \text{ and } D_i = 0 \\ Q_{SB} + Q_{SM} + Q_{GM} & \text{for } S_i=1, G_i=1, \text{ and } D_i = 0 \\ Q_{SB} + Q_{SM} + Q_{GM} + Q_R & \text{for } D_i = 1 \end{cases} \quad (6)$$

416 where, Q is the overall streamflow series, Q_{SB} stands for the baseflow generated by
417 groundwater source, Q_{SM} for snow meltwater runoff, Q_{GM} for glacier meltwater runoff, and
418 Q_R for rainwater directly runoff. The partitioning principles are described as follows:

419 (1) Groundwater is the dominant component ($Q=Q_{SB}$) when both melt and rainwater
420 directly runoff do not occur. This condition requires $S_i=0, G_i=0, \text{ and } D_i=0$;

421 (2) Snow meltwater and groundwater are the dominant components ($Q=Q_{SB}+Q_{SM}$) when
422 the temperature is higher than $0 \text{ }^\circ\text{C}$ at 1650 m a.s.l. and lower than $0 \text{ }^\circ\text{C}$ at 2950 m a.s.l.
423 (requires $S_i=1, G_i=0, \text{ and } D_i=0$);

$$\text{Deleted: } Q = \begin{cases} Q_{SB} & \text{for } S_i+G_i+D_i=0 \\ Q_{SB} + Q_{SM} & \text{for } S_i-G_i-D_i=0 \\ Q_{SB} + Q_{SM} + Q_{GM} & \text{for } G_i-D_i=0 \\ Q_{SB} + Q_{SM} + Q_{GM} + Q_R & \text{else for } D_i=1 \end{cases}$$

Field Code Changed

Deleted:

Deleted: is mathematically equivalent to $S_i+G_i+D_i=0$, which

Deleted: equivalent to $S_i-G_i-D_i=0$, which

428 (3) Snow meltwater and glacier meltwater coupled with groundwater dominate
429 ($Q=Q_{SB}+Q_{SM}+Q_{GM}$) on days when the temperature at 2950 m a.s.l. exceeds 0°C in October to
430 April. This means $G_i=1$, $D_i=0$, and $S_i=1$, noting that S_i must be equal to 1 when $G_i=1$ for the
431 decreasing nature of temperature along altitude;

432 (4) Finally, all sources are mixed ($Q=Q_{SB}+Q_{SM}+Q_{GM}+Q_R$) for other days in the storm
433 rain period (May to September, $D_i=1$). Each category contains days that could be continuous
434 or discontinuous in time and could lie within different weeks due to temporal variability of
435 precipitation and temperature.

436 3.2 Tsinghua Representative Elementary Watershed Hydrological Model

437 The Tsinghua Representative Elementary Watershed model (THREW model) used for
438 the hydrological simulation in this study, has been successfully applied in many watersheds in
439 both China and the United States (see Tian *et al.*, 2008, 2012; Li *et al.*, 2012; Liu *et al.*, 2012
440 etc.), including an application to a high mountainous catchment of Urumqi River basin by
441 Mou *et al.* (2008). The THREW model adopts the REW (Representative Elementary
442 Watershed) approach to conceptualize a watershed, where REW is the sub-catchment unit for
443 hydrological modeling. The study basin was divided into several units (REW) based on a
444 digital elevation model. Sub-catchment units were further divided into a surface and
445 sub-surface layer, each layer containing several sub-zones. The sub-surface layer is composed
446 of two zones: saturated zone and unsaturated zone, and the surface layer consists of six zones:
447 vegetated zone, bare soil zone, snow covered zone, glacier covered zone, sub-stream-network
448 zone, and main channel reach; see Tian *et al.* (2006) for further details.

449 The main runoff generation processes simulated by the THREW model include rainfall
450 surface runoff, groundwater baseflow, snowmelt and glacier melt. Rainfall surface runoff is
451 simulated by a Xin'anjiang module, which adopts a water storage capacity curve to describe
452 non-uniform distribution of water storage capacity of a sub-catchment (Zhao, 1992). The
453 storage capacity curve is determined by two parameters (spatial averaged storage capacity W_M
454 and shape coefficient B). Rainfall surface runoff forms on areas where storage is replete.
455 Replete areas are calculated by the antecedent storage and current rainfall. The saturation
456 excess runoff is computed based on water balance. The remainder of rainfall can infiltrate into
457 soil and become additional contributions to groundwater. Groundwater forms baseflow that is

Deleted: is equivalent to $G_i D_i=1$, which means $G_i=1$, $D_i=0$, and $S_i=1$,

Formatted: Subscript

460 separately calculated by two coefficients (K_A and K_D). K_A and K_D are outflow coefficients of
461 groundwater storage. Their sum determines the flow rate of groundwater baseflow and their
462 ratio (K_D/K_A) dominate the proportion of free groundwater storage. Infiltration and storage
463 should have effects on the calibration of the two parameters. The Xin'anjiang module has
464 been successfully applied to the Qiedeke, Kaidu, Manasi and Kahai basins in Tianshan
465 Mountain by different authors (Jiang, 1987; Yang *et al.*, 1987; Mu and Jiang, 2009), which
466 indicates its applicability in our study area.

467 For the simulation of melt processes in this study, the THREW model was modified to
468 couple with the temperature-index method, given the easy accessibility of air temperature data
469 and generally good model performance of the temperature-index model (Hock, 2003; Singh *et al.*,
470 2000). Snow and glacier melt are simulated using separate degree-day factors (snowmelt
471 degree day factor D_s and glacier melt degree day factor D_g). Glacier melt only occurs in
472 glacier area according to CGI, which remains stable during the study period (2003-2012, see
473 discussion in Sect. 2.2.3). Precipitation in the snow and glacier zone is divided into rainfall
474 and snowfall according to two threshold temperature values (0°C and 2.5°C are adopted in
475 this study according to Wu and Li (2007)), i.e., when temperature is higher than 2.5°C , all
476 precipitation is rainfall, when temperature is lower than 0°C , all precipitation is snowfall, and
477 when temperature falls between the two thresholds, precipitation is divided into rainfall and
478 snowfall half by half (a simple division scheme adopted here). Rainfall on glacier areas forms
479 runoff and flows into the stream-network directly without infiltration into soil. Snow water
480 equivalent (SWE) on glacier areas is updated by combining snowfall and snowmelt, and for
481 simplicity, snow is assumed to cover all glacier areas when the corresponding SWE is not
482 zero. Snowmelt in glacier areas is simulated using snow degree-day factor D_s until it melts
483 away completely. Snow cover area in non-glacier area is updated using MODIS data. To be
484 noted, snowfall in each subcatchment is calculated according to the daily precipitation and
485 temperature. And snowmelt is simulated using the degree-day method. However, the snow
486 water equivalent in the snow cover zone (non-glacier area) is not computed. The existing of
487 snow cover in each subcatchment is only determined by MODIS snow image. When the
488 MODIS image indicates the existing of snow cover and meanwhile the daily temperature is
489 higher than 0°C , then snowmelt will occur, otherwise, snowmelt will not occur. The

Deleted: κ

Formatted: Subscript

Deleted: κ

Formatted: Subscript

492 identification of snow cover by MODIS image is in accordance with the fact that the
493 partitioning of snowmelt dominant hydrograph is based on MODIS snow products. If the
494 existing of snow cover is determined by snow water equivalent, the temperature parameters to
495 calculate snowfall can have significant effects on the estimation of the degree-day factor for
496 snowmelt. To partly reduce this effect, we calibrate the degree-day factor for snowmelt on the
497 basis of MODIS snow cover products. Although in this way, the water balance of snow cover
498 is not taken into account in the snow cover zone, it should not impact the calibration of the
499 degree-day factor for snowmelt. Since MODIS SCA products (i.e., MYD10A2) are available
500 from 2003, the model simulation period is from 2003 to 2012, of which 2003-2007 for
501 calibration and 2008-2012 for evaluation. The time step for simulation is daily.

502 3.3 Stepwise Calibration of Grouped Parameters Upon Partitioning Curves

503 Model parameters are grouped *a priori* according to their connection with causal
504 physical mechanisms (see Table 3). According to Xie *et al.* (2004) and Kang *et al.* (1980),
505 parameters that control groundwater baseflow, snowmelt, glacier melt, and rainwater surface
506 runoff should be the most sensitive parameters for the runoff simulation (also see our
507 sensitivity analysis in Sect. 4.6). These parameters are subjected to calibration in this study.
508 They are related to the corresponding hydrograph parts and then calibrated in a stepwise
509 manner: first, groundwater baseflow parameters (K_b and K_D) are estimated based on the Q_{SB}
510 part of the hydrograph. Second, snowmelt degree day factor (D_s) is calibrated upon the
511 $Q_{SB}+Q_{SM}$ part. Third, glacier melt degree-day factor (D_g) is determined according to the
512 $Q_{SB}+Q_{SM}+Q_{GM}$ part. Finally, rainfall surface runoff parameters (B , W_M) are calibrated on days
513 when D_i equals to 1, i.e., the $Q_{SB}+Q_{SM}+Q_{GM}+Q_R$ part of hydrograph.

514 In each step, only the specific parameter group is subjected to calibration. The
515 parameters determined in the previous steps are kept constant, and all other parameters that
516 will be calibrated in the next steps adopt their initial values. As the simulation in each step can,
517 to some degree, be affected by the initial conditions produced in the preceding step, an
518 iterative procedure is implemented to progressively minimize this influence. The parameter
519 groups are first calibrated based on the corresponding hydrograph parts, and then the stepwise
520 sequence is repeated until the calibrated parameters converge, i.e., the difference in parameter
521 values between two contiguous iterations is less than 10%. In each calibration step, we use

Deleted: κ

Formatted: Subscript

Deleted: κ

Formatted: Subscript

Formatted: Subscript

524 $RMSE_{ln}$ (Eqn. (7), emphasizing low flow) or $RMSE$ (Eqn. (8), emphasizing high flow) as
 525 objective function for parameter optimization. The remaining, insensitive, parameters are
 526 determined *a priori* according to previous modeling experience (mainly from Sun *et al.*
 527 (2012)) and listed in Table 3. The initial values of the calibrated parameters are also
 528 determined *a priori* according to Sun *et al.* (2012) and Tian *et al.* (2012).

529 The overall streamflow can be simulated with all calibrated parameters, which is
 530 evaluated with NSE and NSE_{ln} (logarithm Nash Criterion) values. Given that it is relatively
 531 easier to obtain high evaluation merit values in snowmelt driven basins due to strong
 532 seasonality of streamflow, we further adopt a simple benchmark model (the inter-annual mean
 533 value for every calendar day) to evaluate performance of the proposed method by subtracting
 534 streamflow seasonality. This benchmark model is proposed by Schaepli and Gupta (2007) for
 535 basins having a relatively constant seasonality. The improvement of a model comparing to the
 536 benchmark model is quantified by the BE , see Eqn. (9) for detail.

$$537 \quad RMSE_{ln} = \sqrt{\frac{1}{n} \sum_{i=1}^n (\log Q_{obs}(i) - \log Q_{sim}(i))^2} \quad (7)$$

$$538 \quad RMSE = \sqrt{\frac{1}{n} \sum_{i=1}^n (Q_{obs}(i) - Q_{sim}(i))^2} \quad (8)$$

$$539 \quad BE = 1 - \frac{\sum_{i=1}^n (Q_{obs}(i) - Q_{sim}(i))^2}{\sum_{i=1}^n (Q_{obs}(i) - Q_{ben}(i))^2} \quad (9)$$

540 4 Results and Discussion

541 4.1 Partitioning Hydrographic Curves

542 The hydrograph from 2003 to 2012 was partitioned based on Eqn. (6). In total, we
 543 obtained four kinds of partitioning curves, i.e. Q_{SB} part, $Q_{SB}+Q_{SM}$ part, $Q_{SB}+Q_{SM}+Q_{GM}$ part
 544 and $Q_{SB}+Q_{SM}+Q_{GM}+Q_R$ part. As an example, the partitioning curves in 2003 are shown in Fig.
 545 6, in which the melting period ranges from late February to late November (labeled as red and
 546 green dots). Snowmelt (red dots) starts in February and ends in November, while glacier melt
 547 (green dots) starts later (March) and stops earlier (October). This melt situation agrees well
 548 with the previous studies of Kang *et al.* (1980) and Sun *et al.* (2012). Hydrograph parts
 549 dominated by groundwater source mainly fall into December, January and February and are

550 denoted by black dots. The rainwater surface runoff occurs in the storm rain period only (May
 551 to September, denoted by blue dots). The total number of days of $Q_{SB}+Q_{SM}$ part from 2003 to
 552 2007 is 365, and that of $Q_{SB}+Q_{SM}+Q_{GM}$ part is 249, while the $Q_{SB}+Q_{SM}+Q_{GM}+Q_R$ part
 553 occupies 765 days. The numbers of non-melt days (i.e. the Q_{SB} part, due to glacier melt
 554 generally occurs in the $Q_{SB}+Q_{SM}+Q_{GM}+Q_R$ part) in the five years are 114, 80, 89, 96, and 68,
 555 respectively. Correspondingly, the mean temperatures in those years gauged at the THS are
 556 8.9, 10.1, 9.9, 10.4, and 11.3°C, respectively. A lower mean annual temperature causes a
 557 longer non-melt period in that year and vice versa. Note that the partitioning curves can be
 558 discontinuous in time due to the spatial-temporal variability of temperature.

559 4.2 Model Calibration by the Stepwise Method

560 The six key parameters (K_A , K_D , D_s , D_g , W_M , and B) were firstly calibrated by the
 561 proposed stepwise and iterative method. To focus on baseflow generated by the groundwater
 562 source during the Q_{SB} period, the *RMSEIn* metric that emphasizes low flow is chosen as the
 563 evaluation criterion for the calibration of parameters K_A and K_D . Conversely, high flow is our
 564 focus for the remaining periods ($Q_{SB}+Q_{SM}$, $Q_{SB}+Q_{SM}+Q_{GM}$, $Q_{SB}+Q_{SM}+Q_{GM}+Q_R$) and the
 565 *RMSE* metric is chosen as the evaluation criterion for calibration of parameters D_s , D_g , and
 566 W_M and B . To deal with interaction between steps, an iterative calibration approach was
 567 adopted. A total of five iterations was implemented until the parameter estimates became
 568 stable; the simulation of each kind of partitioning curve in each step of the last iteration is
 569 presented in Fig. 7. The calibrated parameters are shown in Table 4 and the evaluation merits
 570 are listed in Table 5.

571 Figure 7a shows that the magnitude of baseflow in Q_{SB} part was captured well at most of
 572 the times. The *RMSEIn* merit is 0.302 m³/s, and the parameters K_A and K_D were determined as
 573 1.1 and 0.002 respectively. Streamflow in the $Q_{SB}+Q_{SM}$ part is dominated by both snow
 574 meltwater and groundwater. The Fig. 7b shows that melt peak flow events have also been
 575 captured well by a calibrated D_s as 2.5 mm °C⁻¹ day⁻¹ after the determination of K_A and K_D in
 576 the first step. For the $Q_{SB}+Q_{SM}+Q_{GM}$ part, glacier meltwater began to control the streamflow
 577 in combination with snow meltwater and groundwater. Snowmelt and baseflow were
 578 determined *a priori* by previously calibrated parameters. The remaining residual between the
 579 simulated and observed discharge can be attributed to glacier melt alone, which was thus used

Deleted: κ

Formatted: Subscript

Deleted: κ

Formatted: Subscript

Formatted: Subscript

Deleted: κ

Deleted: κ

Formatted: Subscript

Formatted: Subscript

Formatted: Subscript

Deleted: κ

Formatted: Subscript

Deleted: κ

Formatted: Subscript

Deleted: κ

Formatted: Subscript

Deleted: κ

Formatted: Subscript

588 for the calibration of glacier melt factor D_g . The $RMSE$ value for this hydrograph partition
589 was optimized as $4.784 \text{ m}^3/\text{s}$ and we obtained a sound simulation by a calibrated D_g as 7.2
590 $\text{mm } ^\circ\text{C}^{-1} \text{ day}^{-1}$ as shown in Fig. 7c. During the storm rain periods ($Q_{SB}+Q_{SM}+Q_{GM} +Q_R$ part),
591 rainwater directly runoff is an additional important component of river runoff. Similarly,
592 parameters W_M and B can be calibrated separately after *priori* determination of melt runoff
593 and groundwater baseflow. The simulated $RMSE$ value in this period is $12.650 \text{ m}^3/\text{s}$, with
594 calibrated $W_M=10.50 \text{ cm}$ and $B=0.80$. The overall daily streamflow simulation is obtained by
595 combining the four partitions together (see Figure 8a). The corresponding NSE index is 0.881
596 and $NSEln$ is 0.929 . Generally the results suggest a sound simulation compared to the
597 observation.

598 To be noted, the calibrated values of melt degree day factors D_s ($2.5 \text{ mm } ^\circ\text{C}^{-1} \text{ day}^{-1}$) and
599 D_g ($7.2 \text{ mm } ^\circ\text{C}^{-1} \text{ day}^{-1}$) are similar to the values obtained in other studies in Tainshan area, e.g.,
600 D_s is calibrated as $2.5 \text{ mm } ^\circ\text{C}^{-1} \text{ day}^{-1}$ by Liu *et al.* (2012), and D_s and D_g are estimated as 3.1
601 $\text{mm } ^\circ\text{C}^{-1} \text{ day}^{-1}$ and $7.3 \text{ mm } ^\circ\text{C}^{-1} \text{ day}^{-1}$ respectively based on observed mass balance data by Liu
602 *et al.* (1999), which indicates the robustness of our calibration method.

603 4.3 Comparison to Automatic Calibration Method

604 For comparison, we also carry out an automatic calibration with the help of the
605 ε -NSGAI algorithm, an optimization method developed by Deb *et al.* (2002) and Kollat and
606 Reed (2006). The six parameters were calibrated together and evaluated by NSE value of the
607 overall hydrograph. The run time of the automatic algorithm is about 5 weeks (840 hour on a
608 desktop equipped with an Intel Core i7 CPU with 2.8GHz). The NSE value for the final
609 optimized parameters is 0.868 , and the $NSEln$ value is 0.846 (Fig. 8b), both of which are
610 lower than the values obtained by the proposed stepwise method. The parameters calibrated
611 by ε -NSGAI are listed in Table 4, and are different from those calibrated by the stepwise
612 method. Specifically, the snowmelt degree-day factor (D_s) and groundwater baseflow
613 parameters (K_A and K_D) obtained by ε -NSGAI are $2.03 \text{ mm } ^\circ\text{C}^{-1} \text{ day}^{-1}$ and 5.6 and 99.1
614 respectively. The evaluation merits of $RMSE$ and $RMSEln$ for each partitioning curve are also
615 shown in Table 5. In general, the simulation by the automatic algorithm is not as good as that
616 by the stepwise method, especially for the low and middle flow partitions ($Q_{SB}+Q_{SM}$ and
617 $Q_{SB}+Q_{SM} +Q_{GM}$). This may be due to the tendency of NSE-based automatic calibration to

Formatted: Subscript

Formatted: Subscript

Deleted: κ

Formatted: Subscript

Deleted: κ

Formatted: Subscript

620 emphasize high flows.

621 To make a further evaluation, a benchmark model suggested by Schaefli and Gupta
622 (2007) is used for the comparison, which simply simulates daily runoff as the inter-annual
623 daily mean value. Simulation results by the benchmark model are shown in the Figure 8c,
624 which shows *NSE* value as 0.815 and *NSEln* value as 0.923. The high *NSE* and *NSEln* values
625 can be attributed to the strong seasonality of stream discharge in the study basin (Schaefli and
626 Gupta, 2007). The *BE* index (Eqn. (9), see Table 5) is used to measure the improvement of
627 simulations by the calibration methods compared to the benchmark model. A positive value
628 for *BE* means that the evaluated method outperforms the benchmark model. Figure 8 shows
629 the simulations of daily streamflow by the three methods (Fig. 8a by stepwise calibration
630 method, Fig. 8b by automatic calibration method and Fig.8c by benchmark model), which
631 shows better simulation by the two calibration runs with THREW model than the benchmark
632 model (*BE* values are both positive). The stepwise calibration run obtained a *BE* value of
633 0.355, while *BE* of the automatic calibration run is 0.271. The benchmark model describes the
634 mean value of daily discharge on each calendar day. The higher the *BE* value is, the better the
635 seasonal variability of the hydrograph is captured by the evaluation method. The higher *BE*
636 value in the stepwise calibration method can be attributed to the better simulation of middle
637 and low flows which are dominated by groundwater and melt water (Fig.8a). However, *BE*
638 values simulated by two calibrated parameter sets are both relatively low, which is attributed
639 to the poor mimic of the (rapidly rising and falling) peaks.

640 Note that the automatic calibration method based on *NSE* value of the overall
641 hydrograph adopts 1D measurement information to optimize four parameter groups.
642 Benefitting from the partitioning curves, however, the stepwise calibration method increases
643 the dimension of hydrological signature to four. The signature dimension is now equal to the
644 number of parameter groups, and the grouped parameters can be optimized according to their
645 corresponding runoff components separately. A sound simulation of the overall hydrograph is
646 obtained by the reasonable reproduction of the separate partitioning curves. Therefore,
647 parameters calibrated by the stepwise method are inclined to have more explicit physical
648 basis.

649 In regards to computation efficiency, the stepwise calibration required 385 runs of the

Deleted: .

Deleted: measurement information

Deleted: measurement

653 model to complete, with each model run taking about 1.5 minutes and the total computation
654 time being about 10 hrs. In contrast, the state-of-the-art automatic calibration algorithm
655 required about 5 weeks of CPU time consumption on a desktop equipped with an Intel Core
656 i7 CPU and 2.8GHz. The comparison indicates that the stepwise calibration method is both
657 more physically based as well as more computationally efficient.

658 It is worth noting, the performance of the automatic calibration algorithm can increase if
659 the algorithm keeps on running, and even be higher than that of the step-wise calibration
660 method. The comparison here is intending to show that the step-wise calibration method
661 based on hydrograph partition can achieve considerable performance more effectively. The
662 automatic algorithm here treats all the parameters equally during the calibration period. Each
663 parameter should be optimized when searching for the optimal parameter set. This searching
664 algorithm hampers the efficiency of the calibration procedure without identifying the
665 dominant sub-periods for different parameters. In the step-wise calibration method, only
666 parameters that are responsible for the simulation of corresponding hydrograph partition are
667 optimized in each step. And also the calibration of parameter by this method reflects the role
668 of each parameter for the basin runoff generation.

Deleted:

669 4.4 Evaluation for the Stepwise Calibration Method

670 The parameter set calibrated by the stepwise method is applied to the evaluation period
671 (2008~2012), and the daily discharge simulation is shown in Fig. 9a. The evaluation merits
672 are listed in Table 5. The *NSE*, *NSEln* and *RMSE* values for the whole period indicate sound
673 evaluation results but general lower performance compared to calibration period. However,
674 the evaluation results by the stepwise method are still significant better than the benchmark
675 model, which obtained a *NSE* value as low as 0.577 (Fig. 9b and Table 5). The *BE* value in
676 evaluation period by the stepwise calibration method is 0.413. Furthermore, from the partition
677 perspective, the *RMSEln* and *RMSE* values for four partitions in Table 5 show that the low
678 flow simulations (Q_{SB} , $Q_{SB}+Q_{SM}$, and $Q_{SB}+Q_{SM}+Q_{GM}$ parts) are pretty good and even
679 outperform the calibration simulations. The high flow simulation ($Q_{SB}+Q_{SM}+Q_{GM}+Q_R$ part) is,
680 however, insufficient, with *RMSE* 16.727 m³/s (compared to 12.65 m³/s in calibration period).
681 The lower performance of overall evaluation should be attributed to the insufficiency in storm
682 rain days, especially for some extreme storm events in the summer of 2010 (see Fig. 9a). The

684 underestimation of these events is likely due to inadequate observations of rainfall, which are
685 principally due to the strong spatial variability of rainfall in mountainous areas. It is widely
686 acknowledged that the extreme runoff events are difficult to capture in mountain area, where
687 gauged station is scarce, on the daily scale (Aizen *et al.*, 2000; Jasper *et al.*, 2002). However,
688 the accuracy of our results is similar to Li and Williams (2008) (used SRM model) and Liu *et al.*
689 (2012) (who used the MIKE-SHE model) who performed similar work in a basin that is
690 close to TRB in Tianshan Mountains. Their Nash values for daily discharge varied from 0.51
691 to 0.78, and also failed to simulate the peak flows in summer. They also attributed the low
692 efficiency to the heavy precipitation.

693 To further evaluate the robustness of the stepwise calibration method based on
694 partitioning curves, cross validation was implemented. The hydrograph in the evaluation
695 period was partitioned based on dominant runoff sources, as was done in the calibration years
696 2003-2007. We calibrated the model to 2008-2012 and evaluated it for 2003-2007. The new
697 calibrated parameter values are $K_A=0.9$, $K_P=0.003$, $D_s=2.2 \text{ mm } ^\circ\text{C}^{-1} \text{ day}^{-1}$, $D_g=7.4 \text{ mm } ^\circ\text{C}^{-1}$
698 day^{-1} , $W_A=10.2 \text{ cm}$ and $B=0.77$, which are similar to the values calibrated in 2003-2007 listed
699 in Table 4. The *NSE*, *NSEln* and *RMSE* values for calibration period 2008-2012 and
700 evaluation period 2003-2007 are 0.757, 0.900, 10.892 m^3/s and 0.883, 0.910, 8.589 m^3/s ,
701 respectively, using this new calibrated parameter set. The simulations of the two periods by
702 cross validation are presented in Fig.9c-d, which shows similar performance by two calibrated
703 parameter sets and further demonstrates the robustness of the proposed stepwise calibration
704 method.

705 4.5 Sensitivity Analysis on Index-based Partitioning Method

706 The stepwise calibration method relies heavily on the hydrograph partition for different
707 runoff components. The indices defined in Sect. 3.1 are keys to identify the dominant days for
708 melt water and rainwater. The definitions for elevation bands for the 0 °C Isotherm and for
709 storm rain days in the year producing rainwater runoff should have significant influence on
710 the parameter calibration. In this study, the elevation band of 0 °C Isotherm for snowmelt is
711 fixed and defined as 1650m. This value should have minimal effect on the snowmelt
712 simulation, as the occurrence of snowmelt is actually determined by the MODIS snow cover
713 data. Glacier cover area is assumed as constant, which is very rough for we have only one

Deleted: alpine

Deleted: components

Deleted: κ

Formatted: Subscript

Deleted: κ

Formatted: Subscript

Formatted: Subscript

718 CGI data. In this section, we define different elevation bands of 0 °C Isotherm for glacier to
719 analyze the effect of glacier area variation on the model calibration. We also select different
720 seasons as the storm rain period to analyze its sensitive effect.

721 According to the CGI data, the glacier area extends from the altitude of 2950m in 2002.
722 Considering the possible variability, we define four different lowest elevation bands for the
723 glacier area (LEG), i.e., -500m (2450m), -200m (2750m), +200m (3150m) and +500m
724 (3450m). As an example, various hydrograph partition patterns in year 2003 are shown in Fig.
725 10. For the storm rain period (SRP), new seasons are defined as April to October, April to
726 September, May to October, and June to August compared to the benchmark period May to
727 September. A new hydrograph partition pattern in year 2003 is also shown in Fig. 10. The left
728 column in Fig. 10 shows that the $Q_{SB}+Q_{SM}+Q_{GM}$ partition becomes longer while the $Q_{SB}+Q_{SM}$
729 partition becomes shorter when the LEG is lower. Therefore, glacier melt starts earlier and
730 ends later in the years with lower LEG. In the right column, the $Q_{SB}+Q_{SM}+Q_{GM}$ partition
731 becomes longer with the shorter SRP, while the variation of the $Q_{SB}+Q_{SM}$ partition can be
732 negligible. Parameters were re-calibrated according to the new partition curves, and the
733 results are shown in Table 6, indicating the increase of degree-day factor for glacier melt (D_g)
734 with the increase of the LEG. The value of D_g is also found to become higher when the SRP
735 falls in the warmer months. The variation of LEG imposes significant impacts on the
736 calibration of D_g , with a result ranging from 5.8 to 8.0 mm °C⁻¹ day⁻¹, while the variation of
737 SRP principally impacts the calibration of parameter W_M , with a result ranging from 8.2 to
738 10.5 cm. However, the *NSE* values (see Table 6) for different settings show minimal
739 differences. This can be attributed to the fact that parameters are optimized on separate
740 partitioning curves in the stepwise calibration method. Each hydrograph partition can be well
741 simulated by adjusting the parameter values. The partition patterns can influence the value of
742 parameters significantly but only slightly influence the discharge simulation. Among various
743 LEGs, the setting of 2950m leads to the highest *NSE* value. Glacier melt degree day factor (D_g)
744 calibrated with this LEG is 7.2 mm °C⁻¹ day⁻¹, which is very close to the value estimated as
745 7.3 mm °C⁻¹ day⁻¹ by Liu *et al.* (1999), in which the D_g is estimated according to the observed
746 glacier mass balance data in Tianshan area. This can further demonstrate the reasonability of
747 the assumption in Sect. 3.2 that the glacier area is stable and its lowest elevation is fixed at

Formatted: Subscript

748 2950m during the study period. For the various storm rain periods (SRP), when the May to
 749 October period is adopted, the discharge simulation is slightly better than the benchmark
 750 setting of SRP, i.e. May to September. This phenomenon seems to indicate the importance of
 751 precipitation measurement as discussed in Sect. 4.4. Given that the hydrograph partition in
 752 Fig. 6 is on the basis of setting the SRP as May to September, some small rain events in April
 753 are not taken into account. Sensitive analysis in Table 6 indicates that taking these events into
 754 account (i.e., defining SRP as April to October and April to September), the calibrated value
 755 of parameter W_M can be significantly different. With the help of more advanced precipitation
 756 measurement, the storm rain period can be determined more precisely to improve the model
 757 simulation.

758 To evaluate the relative dominance of multiple runoff components on the total runoff, we
 759 compute their contributions to total runoff by various LEG and SRP in Fig.11. The mean
 760 contributions of every runoff component are as follows: groundwater contributes 17%, snow
 761 meltwater contributes 16.5%, glacier meltwater contributes 40% and rainwater directly runoff
 762 contributes 26.5%. Total melt water (snowmelt and glacier melt) occupies approximately 56.5%
 763 and is close to the ratio 63% suggested by Kang *et al.* (1980).

764 4.6 Sensitivity Analysis on Parameters

765 The number of parameters to be calibrated is determined by the parameter sensitivity and
 766 *a priori* analysis. To evaluate the effect of different parameters on the simulation of different
 767 hydrograph partitions, we implemented a simple parameter sensitivity procedure that is
 768 carried out by a “one-at-a-time” approach. Parameters from different groups in Table 3 are
 769 selected for sensitivity analysis, including saturated hydraulic conductivity for u-zone K_u^u ,
 770 saturated hydraulic conductivity for s-zone K_s^s , subsurface flow coefficient K_a and K_p ,
 771 manning roughness coefficient for hillslope n' , spatial heterogeneous coefficient for
 772 infiltration capacity α^{IFL} , ground surface depression storage capacity $Fmax^b$, shape coefficient
 773 to calculate the saturation excess runoff area from the Xin'anjiang model B , spatial averaged
 774 tension water storage capacity in the Xin'anjiang model W_M , glacier degree day factor D_g
 775 and snowmelt degree per day factor D_s . Parameter are varied from -50% to +50% of the
 776 calibrated values using the stepwise method in Table 4. The relative change (R_{MS}) of
 777 simulated measure merits ($RMSEln$ or $RMSE$) for different hydrograph partitions are used to

Formatted: Font: Italic

Formatted: Font: Italic, Subscript

Deleted: K_u^s

Deleted: κ

Formatted: Subscript

Deleted: κ

Formatted: Subscript

Formatted: Subscript

781 evaluate the sensitivity (Eqn. (10)), where MS is the value of measure merits by the calibrated
 782 parameter, MS_+ is the merits value obtained by the parameter +50% of the calibrated one, and
 783 MS_- is the merits value obtained by the parameter -50% of the calibrated one. The sensitivity
 784 simulation results are shown in Table 7, which demonstrates the dominant control of
 785 parameter K_A , K_D , W_M , B , D_s and D_g . Some parameters have significant effects on simulation
 786 of multi hydrograph partitions. For example, parameters controlling the $Q_{SB}+Q_{SM}+Q_{GM}+Q_R$
 787 period can also have significant effect on the other periods. To minimize this interaction,
 788 iterative calibration was implemented in the calibration procedure. The number of calibrated
 789 parameters is determined as six, which control the main runoff components (i.e. groundwater
 790 baseflow, snowmelt, glacier melt and rainwater directly runoff). Note that the low dimension
 791 of parameter calibration should not account for the low efficiency of peak flow simulation,
 792 referring to the similar study in Tianshan mountain areas by Li and Williams (2008), and Liu
 793 *et al.*(2012), in which the models have a higher parameter dimension (higher than six), and
 794 the peak flow simulations are still inadequate.

$$R_{MS} = \left| \frac{MS_+ - MS_-}{MS} \right| \times 100\% \quad (10)$$

796 5 Summary and Conclusion

797 This study proposes a diagnostic calibration approach to extract **hydrological signatures**
 798 from available data series in a **mountain area**, which can be further used to partition the
 799 hydrograph into dominant runoff **sources**. The parameters of a hydrological model were
 800 grouped according to runoff **sources** and then related to the corresponding hydrologic
 801 partitioning curve. Each parameter group was calibrated to improve the simulation of the
 802 corresponding partitioning curve in a stepwise way. In this way, the dimension of
 803 **hydrological signature** is expanded to equal the number of parameter groups. The parameter
 804 uncertainty due to interaction of parameters is reduced via an iterative calibration procedure.
 805 Application to a **mountain watershed** in the Tianshan Mountain in northwestern China
 806 showed that the approach performed reasonably well. Cross validation and comparison to an
 807 automatic calibration method indicated its **applicability**.

808 Note that a semi-distributed hydrological model was utilized to illustrate the proposed
 809 diagnostic calibration approach in the high mountainous Tailan River Basin. Glacier mass
 810 balance is not simulated in the model and the glacier coverage was kept fixed during the study

Deleted: κ

Formatted: Subscript

Deleted: κ

Formatted: Subscript

Formatted: Subscript

Deleted: ing

Deleted: index information

Deleted: n alpine

Deleted: components

Deleted: generation mechanism

Deleted: measurement information

Deleted: an alpine

Deleted: robustness

821 period, which can be subject to significant change in the context of global warming.
822 According to existing studies (Stahl *et al.*, 2008; Schaefli and Huss, 2011; Jost *et al.*, 2012),
823 glacier mass balance data is useful to constrain the parameter uncertainty for hydrological
824 modeling in a glaciated basin. While arguing that our assumption of unchanged glacier
825 coverage will not weaken the importance of the proposed approach, we acknowledge that an
826 improved model coupled with glacier mass balance equations will improve the accuracy of
827 hydrological simulation aided by glacier mass balance observations. This is left for future
828 research.

829 A prerequisite for the proposed approach is hydrograph partitioning based on dominant
830 runoff ~~sources~~. The key to the partition procedure is to identify the functional domain of each
831 runoff ~~source~~, from signature information extracted from easily available data. A partition can
832 be achieved in which the relative roles of different runoff components in the basin runoff vary
833 significantly with time. The ~~mountain~~ watershed is an area in which the runoff ~~source~~ can be
834 separated by the combination of topography, ground-gauged temperature and precipitation,
835 and remotely sensed snow and glacier coverage. Other areas with strong temporal variability
836 of catchment wetness along with precipitation (e.g., monsoon zones) could also be suitable
837 for the proposed approach. The Dunne runoff is prone to dominate the hydrograph when the
838 catchment is wet and it could switch to Hortonian runoff rapidly under the combination of
839 high evaporative demand and less precipitation, as shown by Tian *et al.* (2012) in the Blue
840 River basin of Oklahoma. This is, however, also left for future research.

Deleted: components

Deleted: component

Deleted: alpine

Deleted: components

845 *Acknowledgments.* We wish to thank Mr. Wang Xinhui for his assistance in collecting
846 hydrometeorology data in the Tailan River basin, and thank Charlie Luce and Viviana
847 Lopez-Burgos who provided great help in MODIS snow coverage product filtering. The
848 authors would also like to thank sincerely two Referees (B. Schaefli and M. Zappa) and Editor
849 Markus Weiler for his careful comments, which improve the quality of manuscript significantly.
850 This study was supported by the National Science Foundation of China (NSFC 51190092,
851 U1202232, 51222901) and the foundation of the State Key Laboratory of Hydroscience and
852 Engineering of Tsinghua University (2012-KY-03, 2014-KY-01). Their support is greatly
853 appreciated.

854 **References**

- 855 Ackerman, S. A., Strabala, K. I., Menzel, W. P., Frey, R. A., Moeller, C. C. and Gumley, L.
856 E.: Discriminating clear sky from clouds with MODIS, *J. Geophys. Res.*,103, 32141-32157,
857 1998.
- 858 Aizen, V., Aizen, E., Glazirin, G. and Loaiciga, H. A.: Simulation of daily runoff in Central
859 Asian alpine watersheds, *J. Hydrol.*, 238, 15-34, 2000.
- 860 Akyurek, Z., Surer, S. and Beser, O.: Investigation of the snow-cover dynamics in the Upper
861 Euphrates Basin of Turkey using remotely sensed snow-cover products and
862 hydrometeorological data, *Hydrol. Process.*, 25 (23), 3637-3648, 2011.
- 863 Arnold, J. G. and Allen, P. M.: Automated methods for estimating baseflow and ground water
864 recharge from streamflow records, *Journal of the American Water Resources Association*,
865 35, 411-424, 1999.
- 866 Arnold, J. G., Allen, P. M., Muttiah, R. and Bernhardt, G.: Automated base-flow separation
867 and recession analysis techniques, *Ground Water*, 33, 1010-1018, 1995.
- 868 Beven, K.: Prophecy, reality and uncertainty in distributed hydrological modelling, *Adv.*
869 *Water Resour.*, 16, 41-51, 1993.
- 870 Beven, K.: Equifinality and uncertainty in geomorphological modelling, *The Scientific Nature*
871 *of Geomorphology: Proceedings of the 27th Binghamton Symposium in Geomorphology*,
872 289-313, 1996.
- 873 Beven, K. and Binley, A.: The future of distributed models-model calibration and uncertainty
874 prediction, *Hydrol. Process.*, 6, 279-298, 1992.
- 875 Beven, K. and Freer, J.: Equifinality, data assimilation, and uncertainty estimation in
876 mechanistic modelling of complex environmental systems using the GLUE methodology, *J.*
877 *Hydrol.*,249, 11-29, 2001.
- 878 Blöschl, G., Sivapalan, M., Wagener, T., Viglione, A. and Savenije, H. (Eds.): *Runoff*
879 *Prediction in Ungauged Basins: Synthesis Across Processes, Places and Scales*, Cambridge
880 Univ. Press, New York, 2013.
- 881 Boyle, D. P., Gupta, H. V. and Sorooshian, S.: Toward improved calibration of hydrologic
882 models: Combining the strengths of manual and automatic methods, *Water Resour. Res.*,
883 36, 3663-3674, 2000.
- 884 Brazil, L.: Multilevel calibration strategy for complex hydrologic simulation models, NOAA
885 Technical Report, NWS 42, Fort Collins, 217 pp, 1989.
- 886 Bulygina, N., McIntyre, N. and Wheeler, H.: Conditioning rainfall-runoff model parameters
887 for ungauged catchments and land management impacts analysis, *Hydrol. Earth Syst. Sci.*,
888 13 (6), 893-904, 2009.
- 889 Daly, S. F., Davis, R., Ochs, E. and Pangburn, T.: An approach to spatially distributed snow
890 modelling of the Sacramento and San Joaquin basins, California, *Hydrol. Process*, 14
891 (18SI), 3257-3271, 2000.
- 892 Deb, K., Pratap, A., Agarwal, S. and Meyarivan, T.: A fast and elitist multiobjective genetic
893 algorithm: NSGA-II, *IEEE Transactions on evolutionary computation*, 6, 182-197, 2002.
- 894 Detenbeck, N. E., Brady, V. J., Taylor, D. L., Snarski, V. M. and Batterman, S. L.:
895 Relationship of stream flow regime in the western Lake Superior basin to watershed type
896 characteristics, *J. Hydrol.*, 309, 258-276, 2005.
- 897 Duan, Q., Sorooshian, S. and Gupta, V.: Effective and efficient global optimization for

898 conceptual rainfall-runoff models, *Water Resour. Res.*, 28, 1015-1031, 1992.

899 Dunn, S. M. and Colohan, R. J. E.: Developing the snow component of a distributed
900 hydrological model: a step-wise approach based on multi-objective analysis, *J. Hydrol.*,
901 223, 1-16, 1999.

902 Eder, G., Fuchs, M., Nachtnebel, H. and Loibl, W.: Semi-distributed modelling of the
903 monthly water balance in an alpine catchment, *Hydrol. Process.*, 19, 2339-2360, 2005.

904 Farmer, D., Sivapalan, M. and Jothityangkoon, C.: Climate, soil, and vegetation controls upon
905 the variability of water balance in temperate and semiarid landscapes: Downward approach
906 to water balance analysis, *Water Resour. Res.*, 39, 1035, 2003.

907 Fierz, C., Riber, P., Adams, E., Curran, A., Fohn, P., Lehning, M. and Pluss, C.: Evaluation of
908 snow-surface energy balance models in alpine terrain, *J. Hydrol.*, 282 (1-4), 76-94, 2003.

909 Gafurov, A. and Bardossy, A.: Cloud removal methodology from MODIS snow cover
910 product, *Hydrol. Earth Syst. Sci.*, 13, 1361-1373, 2009.

911 Gan, T. Y. and Biftu, G. F.: Automatic calibration of conceptual rainfall-runoff models:
912 Optimization algorithms, catchment conditions, and model structure, *Water Resour. Res.*,
913 32, 3513-3524, 1996.

914 Gao, W., Li, Z. and Zhang, M.: Study on Particle-size Properties of Suspended Load in
915 Glacier Runoff from the Tomor Peak, *Arid Zone Research*, 28, 449-454, 2011(in Chinese).

916 Gomez-Landesa, E. and Rango, A.: Operational snowmelt runoff forecasting in the Spanish
917 Pyrenees using the snowmelt runoff model, *Hydrol. Process.*, 16, 1583-1591, 2002.

918 Gupta, H. V., Kling, H., Yilmaz, K. K. and Martinez, G. F.: Decomposition of the mean
919 squared error and NSE performance criteria: Implications for improving hydrological
920 modelling, *J. Hydrol.*, 377, 80-91, 2009.

921 Gupta, H. V., Sorooshian, S. and Yapo, P. O.: Toward improved calibration of hydrologic
922 models: Multiple and noncommensurable measures of information, *Water Resour. Res.*, 34,
923 751-763, 1998.

924 Gupta, V. K. and Sorooshian, S.: Uniqueness and observability of conceptual rainfall-runoff
925 model parameters: The percolation process examined, *Water Resour. Res.*, 19, 269-276,
926 1983.

927 Gupta, V. K. and Sorooshian, S.: The Automatic Calibration of Conceptual Catchment
928 Models Using Derivative-Based Optimization Algorithms, *Water Resour. Res.*, 21,
929 437-485, 1985.

930 Gupta, H. V., Wagener, T. and Liu, Y.: Reconciling theory with observations: elements of a
931 diagnostic approach to model evaluation, *Hydrol. Process.*, 22, 3802-3813, 2008.

932 Gurtz, J., Baltensweiler, A. and Lang, H.: Spatially distributed hydrotope-based modelling of
933 evapotranspiration and runoff in mountainous basins, *Hydrol. Process.*, 13, 2751-2768,
934 1999.

935 Haberlandt, U., Klocking, B., Krysanova, V. and Becker, A.: Regionalisation of the base flow
936 index from dynamically simulated flow components - a case study in the Elbe River Basin,
937 *J. Hydrol.*, 248, 35-53, 2001.

938 Hingray, B., Schaefli, B., Mezghani, A. and Hamdi, Y.: Signature-based model calibration for
939 hydrological prediction in mesoscale Alpine catchments, *Hydrolog. Sci. J.*, 55 (6),
940 1002-1016, 2010.

941 Hock, R.: Temperature index melt modelling in mountain areas, *J. Hydrol.*, 282, 104-115,

942 2003.

943 Hooper, R. P. and Shoemaker, C. A.: A Comparison of Chemical and Isotopic Hydrograph
944 Separation, *Water Resour. Res.*, 22, 1444-1454, 1986.

945 Howard, C.: Revisiting the degree-day method for snowmelt computations – Discussion,
946 *Water Resources Bulletin*, 32 (2), 411-413, 1996.

947 Huss, M., Farinotti, D., Bauder, A. and Funk, M.: Modelling runoff from highly glacierized
948 alpine drainage basins in a changing climate, *Hydrol. Process.*, 22 (19SI), 3888-3902, 2008.

949 Jasper, K., Gurtz, J. and Herbert, L.: Advanced flood forecasting in Alpine watersheds by
950 coupling meteorological observations and forecasts with a distributed hydrological model, *J.*
951 *Hydrol.*, 267 (1-2), 40-52, 2002.

952 Jiang, H. F.: Snow ablation modeling and its application to Qiedeke basin, *Journal of*
953 *Xinjiang Agricultural University*, 1, 67-75, 1987 (in Chinese).

954 Johnston, P. R. and Pilgrim, D. H.: Parameter optimization for watershed models, *Water*
955 *Resour. Res.*, 12, 477-486, 1976.

956 Jost, G., Moore, R. D., Menounos, B. and Wheate, R.: Quantifying the contribution of glacier
957 runoff to streamflow in the upper Columbia River Basin, Canada, *Hydrol. Earth Syst. Sci.*,
958 16, 849-860, 2012.

959 Jothityangkoon, C., Sivapalan, M. and Farmer, D. L.: Process controls of water balance
960 variability in a large semi-arid catchment: downward approach to hydrological model
961 development, *J. Hydrol.*, 254, 174-198, 2001.

962 Juston, J., Seibert, J. and Johansson, P.: Temporal sampling strategies and uncertainty in
963 calibrating a conceptual hydrological model for a small boreal catchment, *Hydrol. Process.*,
964 23 (21), 3093-3109, 2009.

965 Kane, D. L., Gieck, R. E., and Hinzman, L. D.: Snow Modeling at Small Alaskan Arctic
966 Watershed, *Journal of Hydrologic Engineering*, 2 (4), 204-210, 1997.

967 Kang, E., Zhu, S. and Huang, M.: Some Results of the Research on Glacial Hydrology in the
968 Region of MT. Tuomuer, *Journal of Glaciology and Geocryology*, 2, 18-21, 1980(in
969 Chinese).

970 Klok, E. J., Jasper, K., Roelofsma, K. P., Gurtz, J. and Badoux, A.: Distributed hydrological
971 modelling of a heavily glaciated Alpine river basin, *Hydrolog. Sci. J.*, 46 (4), 553-570,
972 2001.

973 Kollat, J. B. and Reed, P. M.: Comparing state-of-the-art evolutionary multi-objective
974 algorithms for long-term groundwater monitoring design, *Adv. Water Resour.*, 29, 792-807,
975 2006.

976 Li, H. Y., Sivapalan, M. and Tian, F. Q.: Comparative diagnostic analysis of runoff
977 generation processes in Oklahoma DMIP2 basins: The Blue River and the Illinois River, *J.*
978 *Hydrol.*, 418, 90-109, 2012.

979 Li, X. G. and Williams M. W.: Snowmelt runoff modelling in an arid mountain watershed,
980 *Tarim Basin, China, Hydrol. Process.*, 22 (19SI), 3931-3940, 2008.

981 Liu, D. F., Tian, F. Q., Hu, H. C. and Hu, H. P.: The role of run-on for overland flow and the
982 characteristics of runoff generation in the Loess Plateau, China, *Hydrolog. Sci. J.*, 57,
983 1107-1117, 2012.

984 Liu, S. Y., Xie, Z. C., Wang, N. L. and Ye, B. S.: Mass balance sensitivity to climate change:
985 a case study of glacier no. 1 at Urumqi riverhead, Tianshan mountains, China, *Chin. Geogr.*

986 Sci., 9, 134-140, 1999.

987 Liu, T., Willems, P., Feng, X. W., Li, Q., Huang, Y., Bao, A. M., Chen, X., Veroustraete, F.
988 and Dong, Q. H.: On the usefulness of remote sensing input data for spatially distributed
989 hydrological modelling: case of the Tarim River basin in China, *Hydrol. Process.*, 26 (3),
990 335-344, 2012.

991 Lopez-Burgos, V., Gupta, H. V. and Clark, M.: A probability of snow approach to removing
992 cloud cover from MODIS Snow Cover Area products, *Hydrol. Earth Syst. Sci. Discuss*, 9,
993 13693-13728, 2012.

994 Luo, Y., Arnold, J., Liu, S., Wang, X. and Chen, X.: Inclusion of glacier processes for
995 distributed hydrological modeling at basin scale with application to a watershed in
996 Tianshan Mountains, northwest China, *J. Hydrol.*, 477, 72-85, 2013.

997 Martinec, J., Oeschger, H., Schotterer, U. and Siegenthaler, U.: Snowmelt and groundwater
998 storage in alpine basin, In *Hydrological Aspects of Alpine and High Mountain Areas*,
999 Wallingford, United Kingdom: IAHS Press, 169–175, 1982.

1000 McCuen, R. H.: *Hydrologic analysis and design*, Prentice Hall, New Jersey pp.355-360, 1989.

1001 Mendoza, G. F., Steenhuis, T. S., Walter, M. T. and Parlange, J. Y.: Estimating basin-wide
1002 hydraulic parameters of a semi-arid mountainous watershed by recession-flow analysis, *J.*
1003 *Hydrol.*, 279, 57-69, 2003.

1004 Mou, L., Tian, F., Hu, H. and Sivapalan, M.: Extension of the Representative Elementary
1005 Watershed approach for cold regions: constitutive relationships and an application, *Hydrol.*
1006 *Earth Syst. Sci.*, 12, 565-585, 2008.

1007 Mu, Z. X. and Jiang, H. F.: Establishment of snowmelt type Xin'anjiang watershed model
1008 based on digital elevation model, *Journal of Xinjiang Agricultural University*, 5 (32), 75-80,
1009 2009 (in Chinese).

1010 Nash, J. E. and Sutcliffe, J. V.: River flow forecasting through conceptual models part I — A
1011 discussion of principles, *J. Hydrol.*, 10, 282-290, 1970.

1012 Nathan, R. J., McMahon, T. A.: Evaluation of automated techniques for base flow and
1013 recession analyses, *Water Resour. Res.*, 26, 1465-1473, 1990.

1014 Nejadhashemi, A. P., Shirmohammadi, A., Sheridan, J. M., Montas, H. J. and Mankin, K. R.:
1015 Case Study: Evaluation of Streamflow Partitioning Methods, *J. Irrig. Drain. Eng.*, 135,
1016 791-801, 2009.

1017 Pellicciotti, F., Brock, B., Strasser, U., Burlando, P., Funk, M. and Corripio, J.: An enhanced
1018 temperature-index glacier melt model including the shortwave radiation balance:
1019 development and testing for Haut Glacier d'Arolla, Switzerland, *Journal of Glaciology*, 51
1020 (175), 573-587, 2005.

1021 Pinder, G. F. and Jones, J. F.: Determination of the ground-water component of peak
1022 Determination of the ground-water component of peak discharge from the chemistry of
1023 total runoff, *Water Resour. Res.*, 5, 438-445, 1969.

1024 Rango, A. and Martinec, J.: Application of a Snowmelt-runoff Model Using Landsat Data,
1025 *Nord. Hydrol.*, 10, 225-238, 1979.

1026 Richter, B. D., Baumgartner, J. V., Powell, J. and Braun, D. P.: A method for assessing
1027 hydrologic alteration within ecosystems, *Conservation Biology*, 10, 1163-1174, 1996.

1028 Schaeffli, B. and Gupta, H. V.: Do Nash values have value, *Hydro. Process.*, 21 (15),
1029 2075-2080, 2007.

1030 Schaeffli, B., Hingray, B., Niggli, M. and Musy, A.: A conceptual glacio-hydrological model
1031 for high mountainous catchments, *Hydrol. Earth Syst. Sci.*, 9 (1-2), 95-109, 2005.

1032 Schaeffli, B. and Huss, M.: Integrating point glacier mass balance observations into hydrologic
1033 model identification, *Hydrol. Earth Syst. Sci.*, 15, 1227-1241, 2011.

1034 Shamir, E., Imam, B., Gupta, H. V. and Sorooshian, S.: Application of temporal streamflow
1035 descriptors in hydrologic model parameter estimation, *Water Resour. Res.*, 41, W06021,
1036 doi:10.1029/2004WR003409, 2005a.

1037 Shamir, E., Imam, B., Morin, E., Gupta, H. V. and Sorooshian, S.: The role of hydrograph
1038 indices in parameter estimation of rainfall-runoff models, *Hydrol. Process.*, 19, 2187-2207,
1039 2005b.

1040 Shen, Y., Liu, S., Ding, Y. and Wang, S.: Glacier Mass Balance Change in Tailanhe River
1041 Watersheds on the South Slope of the Tianshan Mountains and its impact on water
1042 resources, *Journal of Glaciology and Geocryology*, 25, 124-129, 2003(in Chinese).

1043 Shi, Y.: Concise Glacier Inventory of China, Shanghai Popular Science Press., Shanghai,
1044 China, 2008(in Chinese).

1045 Singh, P., Kumar, N. and Arora, M.: Degree-day factors for snow and ice for Dokriani
1046 Glacier, Garhwal Himalayas, *J. Hydrol*, 235, 1-11, 2000.

1047 Sivapalan, M., Blöschl, G., Zhang, L. and Vertessy, R.: Downward approach to hydrological
1048 prediction, *Hydrol. Process.*, 17, 2101-2111, 2003.

1049 Sorooshian, S. and Gupta, V. K.: Automatic calibration of conceptual rainfall-runoff
1050 models—the question of parameter observability and uniqueness, *Water Resour. Res.*, 19,
1051 260-268, 1983.

1052 Spear, R. C. and Hornberger, G. M.: Eutrophication in peel inlet—II. Identification of critical
1053 uncertainties via generalized sensitivity analysis, *Water Research*, 14, 43-49, 1980.

1054 Stahl, K., Moore, R. D., Shea, J. M., Hutchinson, D. and Cannon, A. J.: Coupled modelling of
1055 glacier and streamflow response to future climate scenarios, *Water Resour. Res.*, 44, 2008.

1056 Sun, M., Yao, X., Li, Z. and Li, J.: Estimation of Tailan River Discharge in the Tianshan
1057 Mountains in the 21st Century, *Advances on Climate Change Research*, 8, 342-349,
1058 2012(in Chinese).

1059 Swamy, A. N. and Brivio, P. A.: Modelling runoff using optical satellite remote sensing data
1060 in a high mountainous alpine catchment of Italy, *Hydrol. Process.*, 11 (11), 1475-1491,
1061 1997.

1062 Tabony, R. C.: The variation of surface temperature with altitude, *Meteorological Magazine*,
1063 114, 37-48, 1985.

1064 Tahir, A. A., Chevallier, P., Arnaud, Y., Neppel, L. and Ahmad, B.: Modeling
1065 snowmelt-runoff under climate scenarios in the Hunza River basin, Karakoram Range,
1066 Northern Pakistan, *J. Hydrol*, 409, 104-117, 2011.

1067 Tian, F. Q., Hu, H. P. and Lei, Z. D.: Thermodynamic watershed hydrological model:
1068 Constitutive relationship, *Science in China, Ser. E-Technological Sciences*, 51, 1353-1369,
1069 2008.

1070 Tian, F., Hu, H., Lei, Z. and Sivapalan, M.: Extension of the Representative Elementary
1071 Watershed approach for cold regions, *Hydrol. Earth Syst. Sci.*, 10, 619-644, 2006.

1072 Tian, F. Q., Li, H. Y. and Sivapalan, M.: Model diagnostic analysis of seasonal switching of
1073 runoff generation mechanisms in the Blue River basin, Oklahoma, *J. Hydrol*, 418, 136-149,

1074 2012.

1075 Van Griensven, A. and Bauwens, W.: Multiobjective autocalibration for semidistributed
1076 water quality models, *Water Resour. Res.*, 39, 1348, 2003.

1077 Van Straten, G. T. and Keesman, K. J.: Uncertainty propagation and speculation in projective
1078 forecasts of environmental change: A lake-eutrophication example, *J. Forecast.*, 10,
1079 163-190, 1991.

1080 Vivoni, E. R., Entekhabi, D., Bras, R. L. and Ivanov, V. Y.: Controls on runoff generation and
1081 scale-dependence in a distributed hydrologic model, *Hydrol. Earth Syst. Sci.*, 11,
1082 1683-1701, 2007.

1083 Vrugt, J. A., Gupta, H. V., Bastidas, L. A., Bouten, W. and Sorooshian, S.: Effective and
1084 efficient algorithm for multiobjective optimization of hydrologic models, *Water Resour.*
1085 *Res.*, 39, 1214, 2003a.

1086 Vrugt, J. A., Gupta, H. V., Bouten, W. and Sorooshian, S.: A Shuffled Complex Evolution
1087 Metropolis Algorithm for Optimization and Uncertainty Assessment of Hydrological
1088 Model Parameters, *Water Resour. Res.*, 39, 1201, doi:10.1029/2002WR001642, 8., 2003b.

1089 Wang, X. W., Xie, H. J., Liang, T. G. and Huang, X. D.: Comparison and validation of
1090 MODIS standard and new combination of Terra and Aqua snow cover products in northern
1091 Xinjiang, China, *Hydrol. Process.*, 23, 419-429, 2009.

1092 Westerberg, I. K., Guerrero, J. L., Younger, P. M., Beven, K. J., Seibert, J., Halldin, S., Freer,
1093 J. E. and Xu, C. Y.: Calibration of hydrological models using flow-duration curves, *Hydrol.*
1094 *Earth Syst. Sci.*, 15 (7), 2205-2227, 2011.

1095 Wu, J., L. L.: A rain-on-snow mixed flood forecast model and its application, *Engineering*
1096 *Journal of Wuhan University*, 40, 20-23, 2007(in Chinese).

1097 Xie, C., Ding, Y., Liu, S. and Han, H.: Analysis on the Glacial Hydrological Features of the
1098 Glaciers on the South Slope of Mt. Tuomuer and the Effects on Runoff, *Arid Land*
1099 *Geography*, 27, 570-575, 2004(in Chinese).

1100 Yadav, M., Wagener, T. and Gupta, H.: Regionalization of constraints on expected watershed
1101 response behavior for improved predictions in ungauged basins, *Adv. Water Resour.* 30,
1102 1756-1774, 2007.

1103 Yang, D. Q., Zhao, Y. Y., Armstrong, R., Robinson, D. and Brodzik, M. J.: Streamflow
1104 response to seasonal snow cover mass changes over large Siberian watersheds, *J. Geophys.*
1105 *Res.*, 112, F02S22F2, 2007.

1106 Yang, X. S., Jiang, H. F., Huang, C. R. Zheng, Z., and Yong, G.: An applied study on the
1107 snowmelt type of Xin'anjiang watershed model at the Kaidu river basin, *Journal of*
1108 *Xinjiang Agricultural University*, 4, 82-90, 1987 (in Chinese).

1109 Yilmaz, K. K., Gupta, H. V. and Wagener, T.: A process-based diagnostic approach to model
1110 evaluation: Application to the NWS distributed hydrologic model, *Water Resour. Res.*, 44,
1111 W09417, doi:10.1029/2007WR006716, 2008.

1112 Zhang, Z. X., Wagener, T., Reed, P. and Bhushan, R.: Reducing uncertainty in predictions in
1113 ungauged basins by combining hydrologic indices regionalization and multiobjective
1114 optimization, *Water Resour. Res.*, 44 (W00B04), doi:10.1029/2008WR006833, 2008.

1115 Zhao, R. J.: The Xin'anjiang model applied in China, *J. Hydrol.* 135, 371-381, 1992.

1116

Table1. Estimated monthly temperature lapse rate in the TRB

Month	Temperature lapse rate (°C/day/100 m)
January	-0.38
February	-0.38
March	-0.66
April	-0.76
May	-0.80
June	-0.78
July	-0.82
August	-0.86
September	-0.66
October	-0.60
November	-0.54
December	-0.30
Annual	-0.62

1117

1118

Table 2. Estimated week-precipitation lapse rate in storm rain months

Month	Precipitation lapse rate (mm/week/ 100 m)
May	1.63
June	1.69
July	3.14
August	2.40
September	2.28

1119

1120
1121

Table 3. Grouped parameters in the THREW model. Parameters subjected to calibration are highlighted in red.

Category	Symbol	Unit	Description	Value
Subsurface	K_s^u	m s ⁻¹	Saturated hydraulic conductivity for u-zone	1.25E-05
	K_s^s	m s ⁻¹	Saturated hydraulic conductivity for s-zone	1.25E-05
	K_A	-	Coefficient used to calculate subsurface flow	Calibrated
	K_D	-	Coefficient used to calculate subsurface flow	Calibrated
Routing	n^l	-	Manning roughness coefficient for hillslope, obtained from the literature according to land use and vegetation type	1.50E-01
	n^r	-	Similar to n^l , roughness coefficient for channel	3.00E-01
Infiltration	α^{EFL}	-	Spatial heterogeneous coefficient for exfiltration capacity	1.00E+00
	α^{IFL}	-	Spatial heterogeneous coefficient for infiltration capacity	1.50E+00
Interception	$F \max^b$	m	Ground surface depression storage capacity	0.00E+00
	α^{vb}	m	Maximum rainfall depth a single leaf can intercept and hold	1.00E-05
Rainfall runoff	B	-	Shape coefficient to calculate the saturation excess runoff area from the Xin'anjiang model	Calibrated
	W_M	cm	Spatial averaged tension water storage capacity in the Xin'anjiang model	Calibrated
Melt	D_g	mm °C ⁻¹ day ⁻¹	Glacier melt degree day factor	Calibrated
	D_s	mm °C ⁻¹ day ⁻¹	Snowmelt degree day factor	Calibrated

Deleted: κ

Formatted: Subscript

Deleted: κ

Formatted: Subscript

Formatted: Subscript

1122

1125

Table 4. Calibrated parameters by the stepwise and automatic methods

Parameter	Stepwise Calibrated	Automatic Calibrated
K_d	1.1	5.6
K_e	0.002	99.1
D_s (mm °C ⁻¹ day ⁻¹)	2.5	2.03
D_g (mm °C ⁻¹ day ⁻¹)	7.2	7.52
W_M (cm)	10.5	11.9
B	0.80	0.62

1126

Deleted: κ

Formatted: Subscript

Deleted: κ

Formatted: Subscript

Formatted: Subscript

Table 5. Evaluation merits for the stepwise and automatic calibration methods

Merits	Calibration period		Evaluation period		Evaluation period	
	Automatic method	Stepwise method	Benchmark model	Stepwise method	Benchmark model	Benchmark model
$RMSEln(Q_{SB}, m^3/s)$	0.352	0.302	-	0.213	-	-
$RMSE(Q_{SB}+Q_{SM}, m^3/s)$	2.807	1.811	-	1.762	-	-
$RMSE(Q_{SB}+Q_{SM}+Q_{GM}, m^3/s)$	6.079	4.784	-	4.558	-	-
$RMSE(Q_{SB}+Q_{SM}+Q_{GM}+Q_R, m^3/s)$	13.245	12.650	-	16.727	-	-
NSE	0.867	0.881	0.815	0.752	0.577	0.577
$NSEln$	0.841	0.929	0.923	0.894	0.844	0.844
$RMSE (m^3/s)$	8.990	8.459	10.534	11.021	14.381	14.381
BE	0.271	0.355	-	0.413	-	-

1131 Table 6. Sensitive analysis of the calibrated parameters on lowest elevation band for glacier
 1132 area (LEG) and storm rain period (SRP). *NSE* is the Nash Sutcliffe Efficiency value for the
 1133 calibration period.

	LEG (a.s.l. m)	D_s (mm/d/°C)	D_g (mm/d/°C)	W_M (cm)	B	K_A	K_D	λ
SRP: May. To Sep.	3450	2.2	8.0	10.1	0.70	0.7	0.002	Deleted: κ
	3150	2.5	7.9	10.1	0.75	0.7	0.002	Formatted: Subscript
	2950	2.5	7.2	10.5	0.80	1.1	0.002	Deleted: κ
	2750	3.0	6.8	10.2	0.75	1.0	0.002	Formatted: Subscript
	2450	2.8	5.8	10.0	0.78	0.8	0.002	Formatted: Subscript
LEG=2950m	SRP	D_s (mm/d/°C)	D_g (mm/d/°C)	W_M (cm)	B	K_A	K_D	Formatted: Subscript
	Jun. to Aug.	2.9	7.5	8.2	0.75	0.9	0.002	Deleted: κ
	May. to Oct.	2.8	6.9	9.4	0.76	0.8	0.002	Formatted: Subscript
	May. to Sep.	2.5	7.2	10.5	0.80	1.1	0.002	Deleted: κ
	Apr. to Sep.	2.2	7.1	8.3	0.75	0.9	0.002	Formatted: Subscript
Apr. to Oct.	2.6	6.9	9.4	0.77	1.1	0.002	Formatted: Subscript	

1134

1139
1140

Table 7. R_{MS} (%) for parameter sensitivity (R_{MS} values indicating the most sensitive parameters are labeled in bold and red)

Merits	Subsurface		Routing		Infiltration	Interception	Rainfall Runoff		Melt		
	K_s^u	K_s^s	K_A	K_D	n'	α^{IFL}	$F \max^b$	W_M	B	D_s	
<i>RMSE</i> _{In} (Q_{SB})	9.70	11.14	38.44	44.39	15.70	0.12	0.08	1.07	18.51	7.53	
<i>RMSE</i> ($Q_{SB}+Q_{SM}$)	0.32	0.40	11.91	0.06	9.35	0.47	0.14	8.27	25.14	51.22	
<i>RMSE</i> ($Q_{SB}+Q_{SM}+Q_{GM}$)	0.22	0.21	0.62	0.64	10.00	0.17	0.25	7.92	0.29	26.28	
<i>RMSE</i> ($Q_{SB}+Q_{SM}+Q_{GM}+Q_R$)	0.17	0.85	0.57	0.97	1.84	0.08	0.06	19.35	22.48	10.78	11.57

1141

Deleted: *KKA*

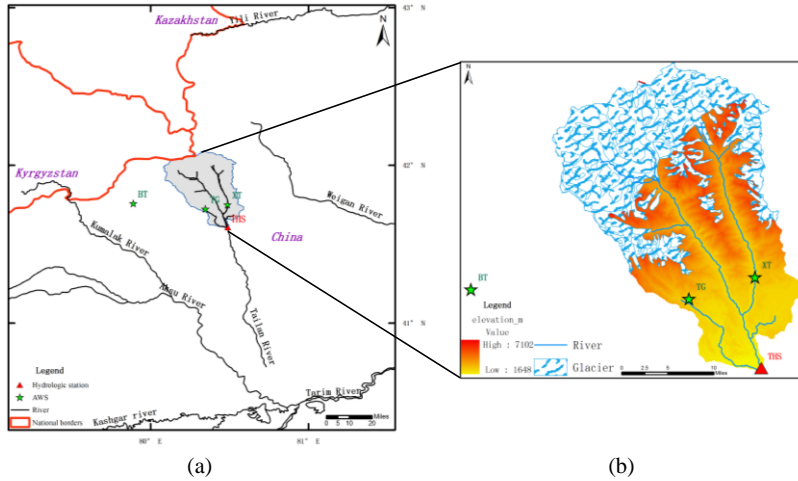
Field Code Changed

Deleted: *KKD*

Field Code Changed

Field Code Changed

Deleted: *WM*

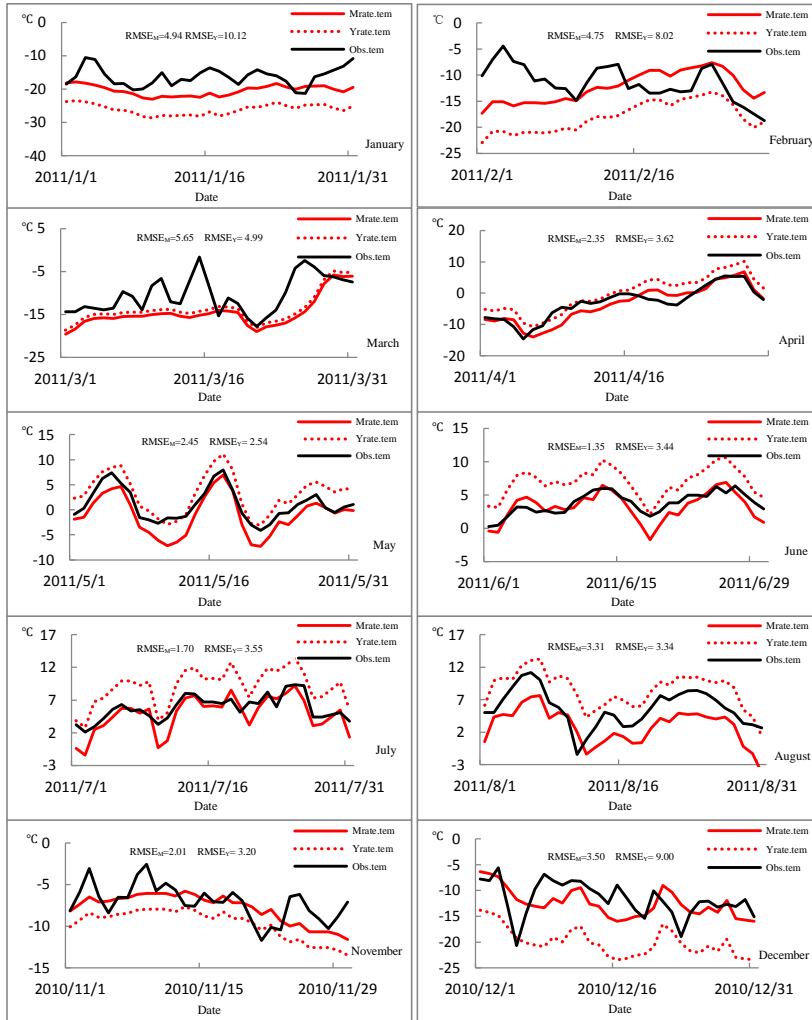


1145
 1146
 1147
 1148
 1149
 1150
 1151
 1152
 1153

(a) (b)

Figure 1. Location of the Tailan River basin in Xinjiang Uygur Autonomous Region, China. Two automatic weather stations (TG at 2381 m a.s.l. and XT at 2116 m a.s.l.) were set up in upstream mountain area in July, 2011. Additionally, the BT weather station (3950 m a.s.l.) located in the adjacent Kumalak River basin was used to validate the estimated temperature lapse rates. The Tailan Hydrologic Station (THS) has gauged streamflow data at the catchment outlet since 1957(a).Glacier occupies approximately 33% of the total basin area (b).

1154



1158

1159

1160

1161

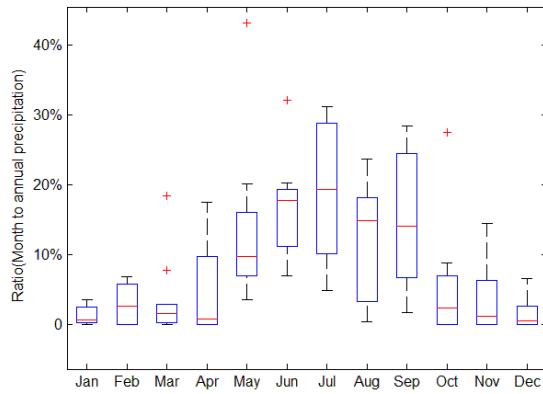
1162

1163

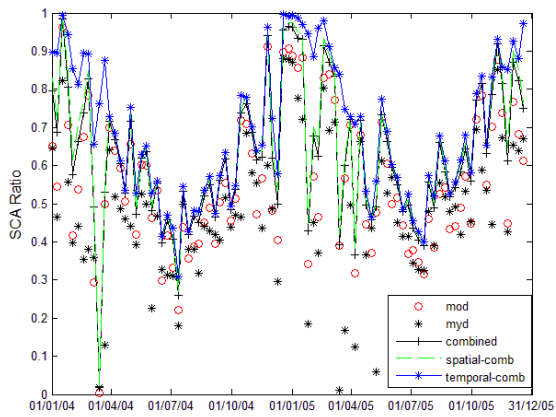
1164

1165

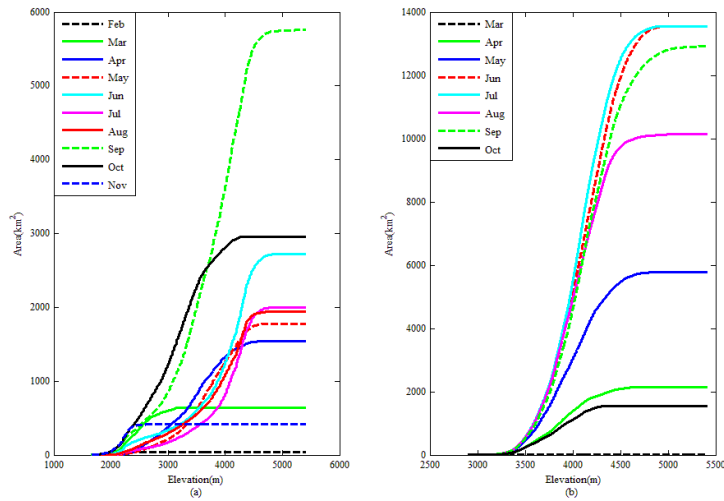
Figure 2. Evaluation of the estimated temperature lapse rate at the BT station. The black solid line is the observed temperature series at BT (Obs.tem); the red solid line is the estimated temperature by monthly lapse rate (Mrate.tem). The red dotted line indicates the estimated temperature based on annual constant rate (Yrate.tem). The goodness of fit between the observed and estimated temperature is measured by $RMSE_M$ for monthly lapse rate and $RMSE_Y$ for annual constant rate, respectively. The temperature series in September and October are absent at BT.



1166
 1167 Figure 3. Proportion of monthly precipitation to annual amount (2003~2012). The red line in
 1168 each box represents the median value for each month from 2003 to 2012. Red crosses indicate
 1169 abnormal values that exceed 1.5 times the inter quartile range.

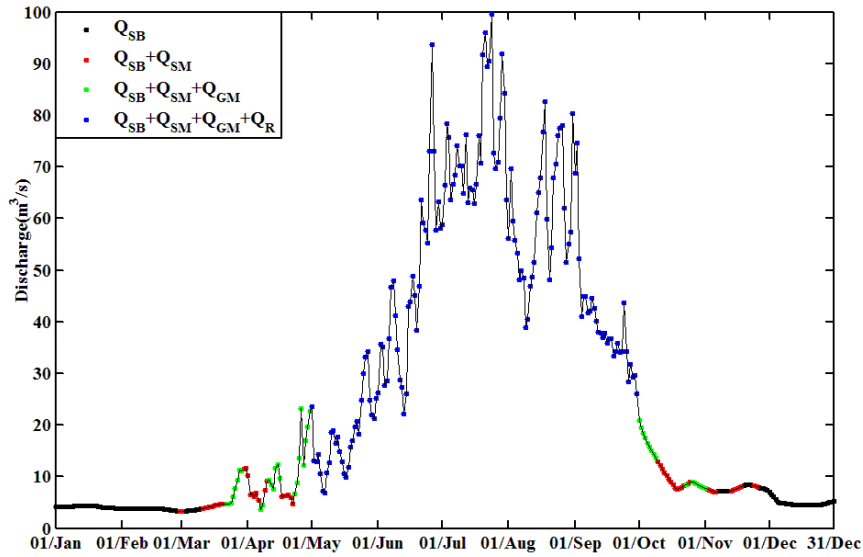


1170
 1171 Figure 4. Filtered MODIS eight-day snow-cover products (2004-2005). The term 'mod' is the
 1172 snow cover area from MOD10A2 products, 'myd' is MYD10A2 products, 'combined' is the
 1173 combined result from step1, 'spatial-comb' from step2 and 'temporal-comb' from step3. See
 1174 Sect. 2.2.3 for details.



1175
 1176
 1177
 1178
 1179
 1180

Figure 5. Altitudinal Cumulative Melt Curve. (a) Cumulative monthly snowmelt area distribution by elevation (2003~2012). (b) Cumulative monthly glacier melt area distribution by elevation (2003~2012). The snowmelt areas in December and January and the glacier melt areas in November, December, January and February are zero and are not shown in this figure.



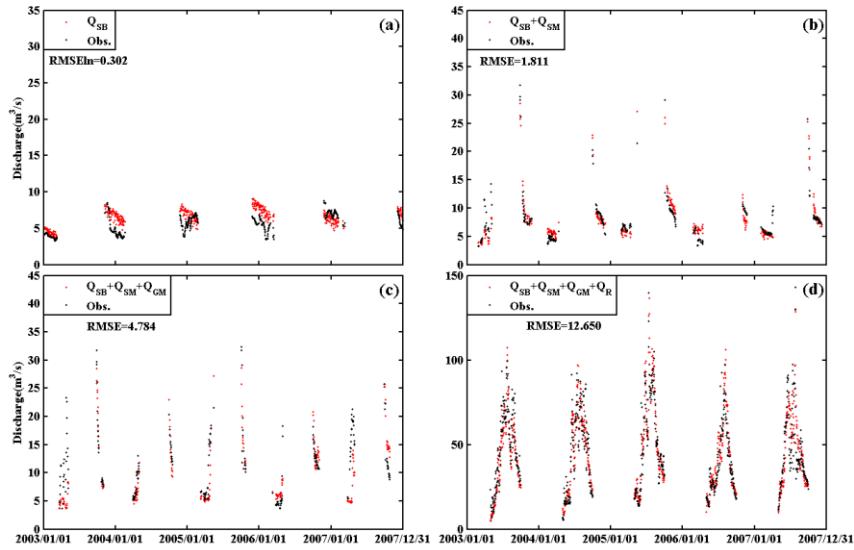
1181

1182

1183

1184

Figure 6. Hydrograph partition in 2003. Q_{SB} stands for subsurface baseflow generated by groundwater, Q_{SM} and Q_{GM} for snow meltwater and glacier meltwater respectively, and Q_R for rainwater directly runoff.



1185

1186

1187

1188

1189

1190

1191

Figure 7. Stepwise calibration of grouped parameters upon partitioning curves. (a) Partitioning curves after calibrating K_A and K_D upon Q_{SB} . (b) Partitioning curves after calibrating D_s upon $Q_{SB}+Q_{SM}$. (c) Partitioning curves after calibrating D_g upon $Q_{SB}+Q_{SM}+Q_{GM}$. (d) Partitioning curves after calibrating W_M and B upon $Q_{SB}+Q_{SM}+Q_{GM}+Q_R$. The goodness of fit between observed and simulated discharge is measured by $RMSEln$ (for Q_{SB} part) or $RMSE$ (for other parts).

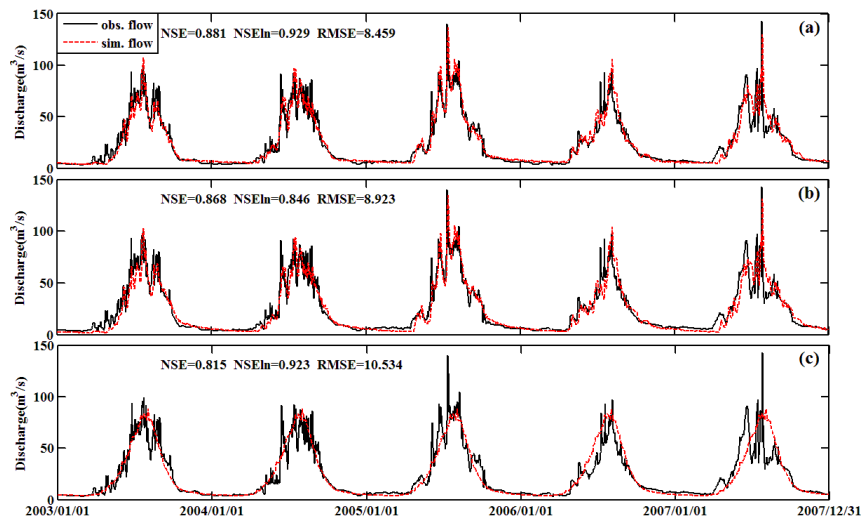
Deleted: κ

Formatted: Subscript

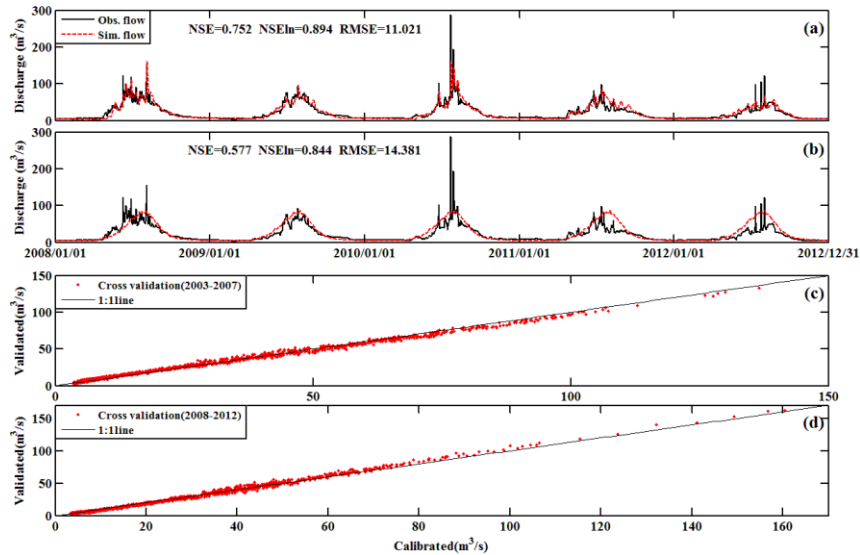
Deleted: κ

Formatted: Subscript

Formatted: Subscript



1194
 1195 Figure 8. Simulation of daily streamflow by different methods from 2003 to 2007. (a) by the
 1196 proposed stepwise method, (b) by the automatic calibration method, and (c) by the benchmark
 1197 model. The performance of the simulations is measured in NSE , $NSEln$ and $RMSE$.



1198

1199

1200

1201

1202

1203

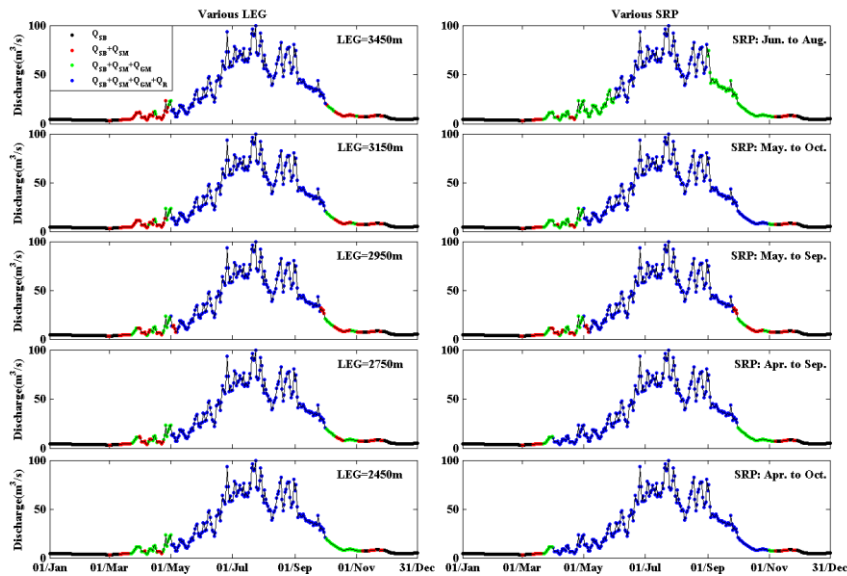
1204

1205

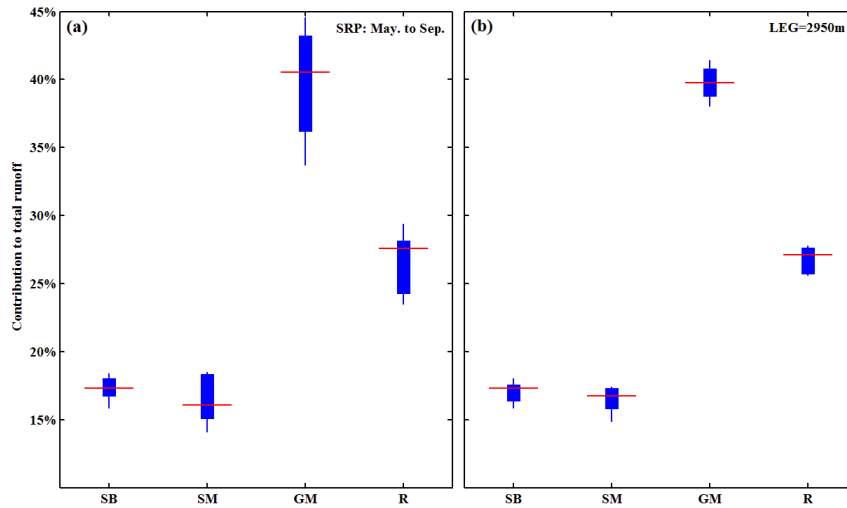
1206

1207

Figure 9. Evaluation of the stepwise calibration method. (a) discharge simulation in evaluation period 2008 to 2012 using the stepwise calibrated parameters in calibration period 2003 to 2007. (b) discharge simulation in evaluation period 2008 to 2012 by the benchmark model. (c) Cross validation simulation of daily discharge in 2003-2007. x-coordinate presents the simulated daily discharges by parameters calibrated in period 2003-2007. y-coordinate presents the simulated daily discharges by parameters calibrated in period 2008-2012. (d) Cross validation simulation of daily discharge in 2008-2012. x-coordinate presents the simulated daily discharges by parameters calibrated in period 2008-2012. y-coordinate presents the simulated daily discharges by parameters calibrated in period 2003-2007.



1208
 1209 Figure 10. Sensitivity analysis for hydrograph partition. The first column is the hydrograph
 1210 partition pattern using different lowest elevation band of the glacier area (LEG). The second
 1211 column is the hydrograph partition pattern using different storm rain period (SRP).
 1212



1213
 1214
 1215
 1216
 1217
 1218
 1219
 1220

Figure 11. Sensitivity analysis on the contributions of different runoff sources to total runoff. (a) is the contribution pattern under different lowest elevation band of glacier area (LEG), where the storm rain period (SRP) is fixed as May to September. (b) is the contribution pattern under different SRPs, where the LEG is fixed as 2950m. The red line stands for the mean contribution for each runoff source, and the top/bottom end of each plot presents the highest/lowest contribution ratio. SB is groundwater baseflow, SM is snowmelt, GM is glacier melt and R is rainwater directly runoff.

Deleted: components

Deleted: component